Gondwana Research 111 (2022) 76–94

Contents lists available at ScienceDirect

Gondwana Research

journal homepage: www.elsevier.com/locate/gr

Rapid early Permian tectonic reorganization of Laurentia's plate margins: Evidence from volcanic tuffs in the Permian Basin, USA

Hepeng Tian [a], Majie Fan [a,*], Victor Valencia [b], Kevin Chamberlain [c], Lowell Waite [d], Robert J. Stern [d], Matthew Loocke [e]

[a] Department of Earth and Environmental Sciences, University of Texas at Arlington, United States
[b] School of Environment, Washington State University, United States
[c] Department of Geology and Geophysics, University of Wyoming, United States
[d] Department of Geosciences, University of Texas at Dallas, United States
[e] Department of Geology and Geophysics, Louisiana State University, United States

ARTICLE INFO

Article history:
Received 5 November 2021
Revised 31 May 2022
Accepted 5 July 2022
Available online 11 July 2022
Handling Editor: R.D. Nance

Keywords:
CA-ID-TIMS
LA-ICPMS
Zircon
Pangea
Magmatic arc
Permian Basin
Volcanic tuff

ABSTRACT

Early Permian arc magmatism is critical to understanding the final assembly of the supercontinent Pangea and subsequent plate reorganization. Here we report the geochronology and geochemistry of Cisuralian and Guadalupian volcanic tuffs in southwestern Laurentia and infer the magmatic sources and plate reorganization related to Laurentia-Gondwana collision. Zircon CA-ID-TIMS U-Pb dates of tuffs in the Wolfcamp B, Wolfcamp A and lower Spraberry units in the Permian Basin provide the first set of absolute ages of Cisuralian deposits in this basin. Zircon geochemistry data further show that the parent melts of these tuffs were granitic melts that formed in continental arcs. Syn-depositional zircons from the Wolfcamp B tuff beds (288.2 ± 1.7 Ma) have an average ε_{Hf} value of +5.5 and T_{DM2} model ages between 675 and 1207 Ma, reflecting a mixture of juvenile mantle melts and Precambrian crust. The isotopic signature is consistent with Mississippian Laurentian tuffs derived from a northern Gondwana arc formed by the subduction of the Rheic oceanic plate. However, zircons from a Wolfcamp A tuff bed (287.2 ± 0.5 Ma) show an average ε_{Hf} value of −4.5, much more evolved than the inferred northern Gondwana arc, but consistent with granitoids of similar or younger age in the Oaxaquia terrane. This change in ε_{Hf} most likely reflects magmatism related to subduction of a paleo-Pacific oceanic plate beneath western Pangea. Our interpretation suggests a late Cisuralian plate reorganization that was caused by plate reorganization following Pangea assembly led to rapid (~1 Myr) initiation of subduction beneath western Pangea. This study also compares tuff dates from LA-ICPMS and CA-ID-TIMS U-Pb dating and concludes that the weighted mean date of the youngest dominant KDE mode (WMYDM) is the best way to approximate LA-ICPMS dates to true depositional ages.

1. Introduction

1.1. Late Paleozoic tectonics

Plate reorganizations, as natural consequences of plate tectonics, are difficult to recognize in the pre-Jurassic geologic record. The driving forces of plate reorganization are derived principally from mantle convection or plates with dynamic feedback between the two (e.g., Anderson, 2001; King et al., 2002; Matthews et al., 2012; Mallard et al., 2016). Major plate reorganizations that took as short as less than a few million years are thought to be less likely caused by mantle buoyance forces due to oceanic slab subduction, ocean plate thickening, or upwelling of mantle plume. They are more likely caused by changes in plate motion due to creation of new or destruction of old plate margins (Richards and Lithgow-Bertelloni, 1996). The rates of plate reorganization in the last 200 Myr, with less uncertainty for the last 100 Myr, are traditionally determined from analysis of ocean-floor magnetic lineations (e.g., Morra et al., 2013); this approach is not possible before the Jurassic because older seafloor has been subducted. The sparsity of geologic evidence for the rate of plate reorganization > 200 Myr limits our understanding of plate tectonic history and assessment of the geodynamic drivers of plate reorganizations.

* Corresponding author.
E-mail addresses: hepeng.tian@uta.edu (H. Tian), mfan@uta.edu (M. Fan), kchamber@uwyo.edu (K. Chamberlain), Lowell.Waite@utdallas.edu (L. Waite), rjstern@utdallas.edu (R.J. Stern), mloock1@lsu.edu (M. Loocke).

https://doi.org/10.1016/j.gr.2022.07.003
1342-937X/

Plate reorganization associated with assembly of the supercontinent Pangea is undoubtedly an important late Paleozoic tectonic event. Subduction of the Rheic plate beneath northern Gondwana may have started during the Early Mississippian (e.g., Estrada-Carmona et al., 2016; Tian et al., 2022; Zhao et al., 2020), as early as ~348 Ma (Ramírez-Fernández et al., 2021). The assembly of Pangea was marked by closure of the Rheic ocean, accretion of *peri*-Gondwanan terranes to Laurentia, and diachronous Laurentia-Gondwana collision to form the Appalachian-Ouachita-Marathon-Sonora orogenic belt (e.g., Nance and Linnemann, 2008; Domeier and Torsvik, 2014). The collision destroyed the intervening subduction zone(s), ultimately leading to subduction of the Paleo-Pacific oceanic plate beneath western Pangea. However, details about the change from Rheic oceanic plate to Paleo-Pacific oceanic plate subduction are poorly understood. The lack of understanding, in part, reflects the fact that arc magmatic products (esp. granitic rocks) related to Rheic ocean subduction may have been overprinted by those related to the eastward subduction of the Paleo-Pacific oceanic plate beneath western Pangea. Torres et al. (1999) proposed that a Permian-Triassic (287–232 Ma) continental arc in eastern Mexico (the East Mexico arc) was likely caused by eastward subduction of the Paleo-Pacific oceanic plate beneath western Gondwana and claimed that this arc may have extended into California, USA. This inference is supported by arc magmatism that initiated as early as early Permian (275 Ma) in the Mojave Desert, southern California, USA (Cecil et al., 2019) as well as the dominant ~274 Ma zircon age cluster in the Permian Monos Formation deposited in a forearc setting in northwestern Sonora, Mexico (Dobbs et al., 2021). Moreover, Kirsch et al. (2012) and Ortega-Obregón et al. (2014) suggested that the Permian-Triassic arc, related to subduction of the Paleo-Pacific oceanic plate, may have started during the Pennsylvanian (311 Ma) in southern Mexico. An alternative model is that the early Permian plutonic and volcanic rocks in southern, central and northern Mexico represent the southwestern extension of Rheic oceanic plate subduction beneath western Gondwana due to the preservation of Rheic ocean vestiges and lack of Triassic magmatic units related to subduction of the Paleo-Pacific oceanic plate in the region (e.g., Elías-Herrera and Ortega-Gutiérrez, 2002; Vega-Granillo et al., 2007, 2009; Ortega-Gutiérrez et al., 2018; Zúñiga et al., 2020). Consequently, Permian magmatic units in Mexico south of the Marathon-Sonora belt are interpreted as either products of Paleo-Pacific or Rheic oceanic plate subduction (e.g., Keppie et al., 2008; Nance et al., 2010; Ortega-Obregón et al., 2014; Rosales-Lagarde et al., 2005; Coombs et al., 2020). Therefore, studies of early Permian magmatic units near the west terminus of the Laurentia-Gondwana collisional belt are important for understanding the change from one subduction system to the other and the evolution of magmatism related to Pangea assembly.

1.2. Permian Basin chronostratigraphy

The Permian Basin of western Texas and southeastern New Mexico contains thick Paleozoic sedimentary rocks that record the last stages in the late Paleozoic assembly of Pangea (e.g., Ross, 1986; Yang and Dorobek, 1995; Liu and Stockli, 2020). Despite many decades of study by especially industry geoscientists, the ages of basin-fills are poorly constrained because of the lack of isotopic dates and the scarcity of paleontological studies. Age constraints for early and middle Permian (Cisuralian and Guadalupian) series in the subsurface of the basin are mostly based on subsurface correlations to the outcrop type sections in the Glass and Guadalupe Mountains, western Texas, respectively (e.g., Silver and Todd, 1969; Handford, 1981; Mazzullo and Reid, 1989; Hamlin and Baumgardner, 2012; Baumgardner et al., 2016). The chronostratigraphy of Cisuralian type sections are based on the correlation of microfossils to the sections with Global Boundary Stratotype Section and Point (GSSP) where absolute ages are constrained by isotopic dating of tuffs (Behnken, 1984; Wardlaw and Davydov, 2000; Ross and Ross, 2003; 2009; Wahlman, 2013; Wardlaw and Nestell, 2014). Few microfossil studies have been conducted in the Cisuralian series of the Permian Basin and are focused on deep-water deposits in the northern part of the basin (Wahlman et al., 2016; Kohn et al., 2019). These sites are unsuitable for basin-wide stratigraphic correlation, which is a common practice of chronostratigraphic correlation to constrain the depositional ages of other sites, because these deposits were disturbed by episodic debris flows (Baumgardner et al., 2016) and fossils at shallow depth may have been later mixed into deep-water deposits. Additionally, microfossil studies in western Texas have mostly followed the North America Permian regional time scale defined by fusulinids while the International Time Scale for the Permian Period was defined by conodonts and isotopic dates (Chernykh and Ritter, 1997; Davydov et al., 1998; Chuvashov et al., 2002; Chernykh et al., 2006; Chuvashov et al., 2013). The use of different microfossils prevents a direct correlation between the North America Permian regional time scale with the International Permian Scale.

Here we report whole rock geochemistry, zircon U-Pb geochronology using both CA-ID-TIMS and LA-ICPMS, and zircon hafnium isotope and trace element geochemistry of 12 late Paleozoic volcanic tuffs (~288 to ~280 Ma) preserved in the Permian Basin and the Guadalupe Mountains north of the Marathon orogenic belt (Fig. 1). These data are used to 1) constrain tuff ages and refine the chronostratigraphy of lower Permian strata in the Permian Basin; 2) understand the magmatic affinity and sources of these tuffs; and 3) unravel tectonic processes during the final collision of Laurentia and Gondwana near the western edge of the central Pangea suture. Our results have implications for best practices in statistical analysis of LA-ICPMS dates for age determination and the rate of plate reorganization.

2. Geologic background

The Permian Basin is located in western Texas and southeastern New Mexico, USA. It is over 400 km across and is one of the largest sedimentary basins in North America. It is bounded by the Marathon-Ouachita fold-and-thrust belt to the south, the Diablo Platform to the west, the Northwestern Shelf to the northwest, the Northern Shelf to the north and the Eastern Shelf to the east (Fig. 1). The Basin is subdivided into the Delaware Basin in the west and the Midland Basin in the east, separated by the Central Basin Platform. The region was part of a broad continental basin on the southern Laurentian passive margin from Early Ordovician to Late Mississippian time, known as the Tobosa Basin, and was reshaped and structurally differentiated during the Carboniferous-early Permian by NNW-SSE trending Ancestral Rocky Mountain structures to the north (Leary et al., 2017) and the Laurentia-Gondwana collision to the south (Ross, 1986). It is generally thought that the collision began in the Appalachians during the Late Mississippian and propagated westward to the Ouachita Mountains in Arkansas and Oklahoma in the Early Pennsylvanian and ended in the Marathon region in western Texas and Sonora by the early Permian (Poole et al., 2005).

During the passive margin stage, the Tobosa Basin was in a marine depositional environment and accommodated nearly 1 km of siliciclastic and carbonate rocks with minor carbonate turbidites. The sequence includes Lower Ordovician sandstones and shales, overlain by Middle-Upper Ordovician, Silurian, Middle Devonian, and Mississippian carbonates with subordinate siliciclastic rocks, and the Upper Devonian and Lower Mississippian Woodford Shale (e.g., Adams, 1965; Ross, 1986; Dutton et al.,

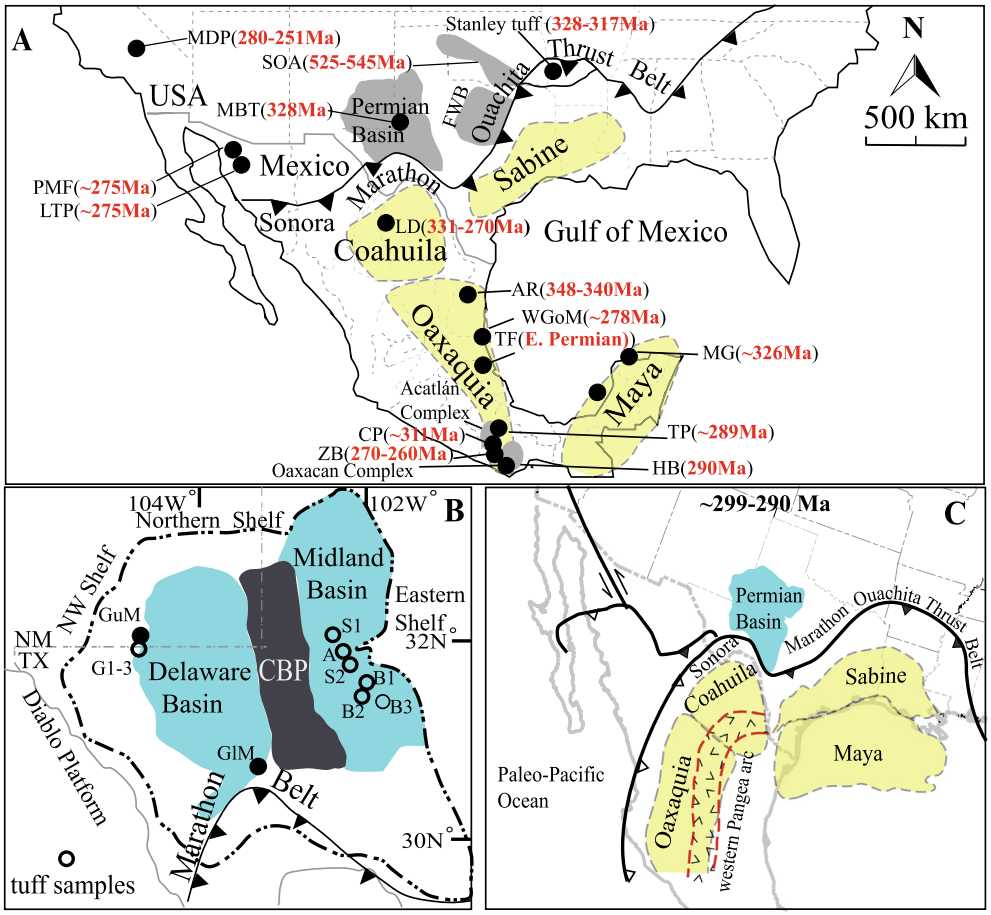

Fig. 1. Simplified geologic map of A) southern North America showing the locations of Peri-Gondwana terranes, the Ouachita-Marathon-Sonora fold and thrust belt, the Permian Basin, and the tuff sources discussed in the paper. AR: Aserradero Rhyolite (Ramírez-Fernández et al., 2021); CP: Cuanana pluton (zircon ε_{Hf} between +3 and +9; Ortega-Obregón et al., 2014); FWB: Fort Worth Basin; HP: Honduras batholith (zircon ε_{Hf} values between +5 and +8; Ortega-Obregón et al., 2014); LD: Las Delicias arc (whole rock ε_{Nd} between +2.6 and +5.3; Lopez, 1997); LTP: Los Tanques pluton (zircon ε_{Hf} signature of ~−7.5; Riggs et al., 2016); MDP: Mojave Desert pluton (zircon ε_{Hf} between −5 and +10 for 280–260 Ma zircon grains; Cecil et al., 2019); MT: Mississippian Barnett tuff in the Midland Basin (zircon ε_{Hf} of between 0 and +5; Tian et al., 2022); PMF: Permian Monos Formation (Dobbs et al., 2021); MG: Early Mississippian granitoids (zircon ε_{Hf} between +3.8 and +6.0; Zhao et al., 2020); SOA: Southern Oklahoma Aulacogen (Thomas et al., 2016); TP: Totoltepec pluton (whole rock ε_{Nd} between −0.8 and +2.6; Kirsch et al., 2012); TF: lower Permian Tuzancoa Formation (whole rock εNd of +4.4; Rosales-Lagarde et al., 2005); WGoM: western Gulf of Mexico (zircon ε_{Hf} of −6.0; Coombs et al., 2020); ZB: Zaniza batholith (zircon ε_{Hf} between −14 and −1; Ortega-Obregón et al., 2014). B) Map showing the Permian Basin the studied volcanic tuffs in the basin. CBP: Central basin platform; GlM: Glass Mountains; GuM: Guadalupian Mountains. C) Paleogeographic map of southern Laurentia and northern Gondwana at ~299–290 Ma. The figure is modified after Lawton et al. (2021). Black triangles represent orogenic front and white triangles represent convergent plate margin. To the northwest of Sonora, arc magmatism in the Caborca Block was approximately coeval with the Sonora orogeny, suggesting the onset of subduction of paleo-Pacific plate beneath Caborca during this time may have caused the inception of Cordilleran arc (Lawton et al., 2021).

2005). The pre-collision Upper Mississippian to Middle Pennsylvanian sedimentary rocks in the Permian Basin are characterized by thinly bedded limestone, shale and sandstone that were deposited in a shallow-marine environment (Ross, 1986). During the Late Pennsylvanian to early Permian collision, the Basin experienced rapid flexural subsidence, thrust faulting, and major glacioeustactic sea-level changes (Crowell, 1978), and accommodated a thick section (~4.2 km) of deep-marine shale and turbidite deposits that overlie the Lower Ordovician-Middle Pennsylvanian marine siliciclastic and carbonate rocks (Ross, 1986). The deepwater depositional environment persisted until the end of Guadalupian before the basin was blanketed by upper Permian evaporites (Silver and Todd, 1969).

Nine Cisuralian volcanic tuffs were collected from subsurface cores in the Midland Basin where the total thickness of Permian strata is about 1.5–2.0 km (Hill, 1996). Adams et al. (1939) first divided the Permian strata in the Permian Basin into four North America stages based on biostratigraphy and lithology, including the Wolfcampian, Leonardian, Guadalupian and Ochoan (Fig. 2). Permian strata in the Glass Mountains, to the south of the Delaware Basin (Fig. 1), is a continuous and complete succession from the base of the Wolfcampian stage to the top of the Guadalupian stage and is considered as the type section of Permian strata in North America (Hill, 1996). Stratigraphic correlations of Permian strata between the subsurface of the Midland Basin and Glass Mountains exposures are mainly by lithology (Ross, 1986; Yang and Dorobek, 1995; Hill, 1996) with a few biostratigraphic constraints from Kohn et al. (2019). In the Glass Mountains, Wolfcampian sedimentary rocks mainly consist of shale and limestone; Leonardian rocks are shale with thin beds of limestone; Guadalupian rocks are mainly limestone; and Ochoan rocks are massive evaporites (Adams, 1965).

The subsurface lithostratigraphic nomenclature in the Permian Basin is not synonymous with the formal chronostratigraphic intervals from Glass Mountains type sections but evolved to serve hydrocarbon exploration purposes. Early Permian Wolfcampian operational units include the Wolfcamp Shale, which is subdivided into A, B, C and D units, from top to bottom (Fig. 2). Microfossil studies and stratigraphic correlations have shown that the Wolfcamp D unit is Late Pennsylvanian (Baumgardner et al, 2016) while the Wolfcamp A is early Leonardian (Wilde, 1975; Mazzullo, 1982; Mazzullo et al., 1987; Mazzullo and Reid, 1989; Wilde, 1990). Kohn

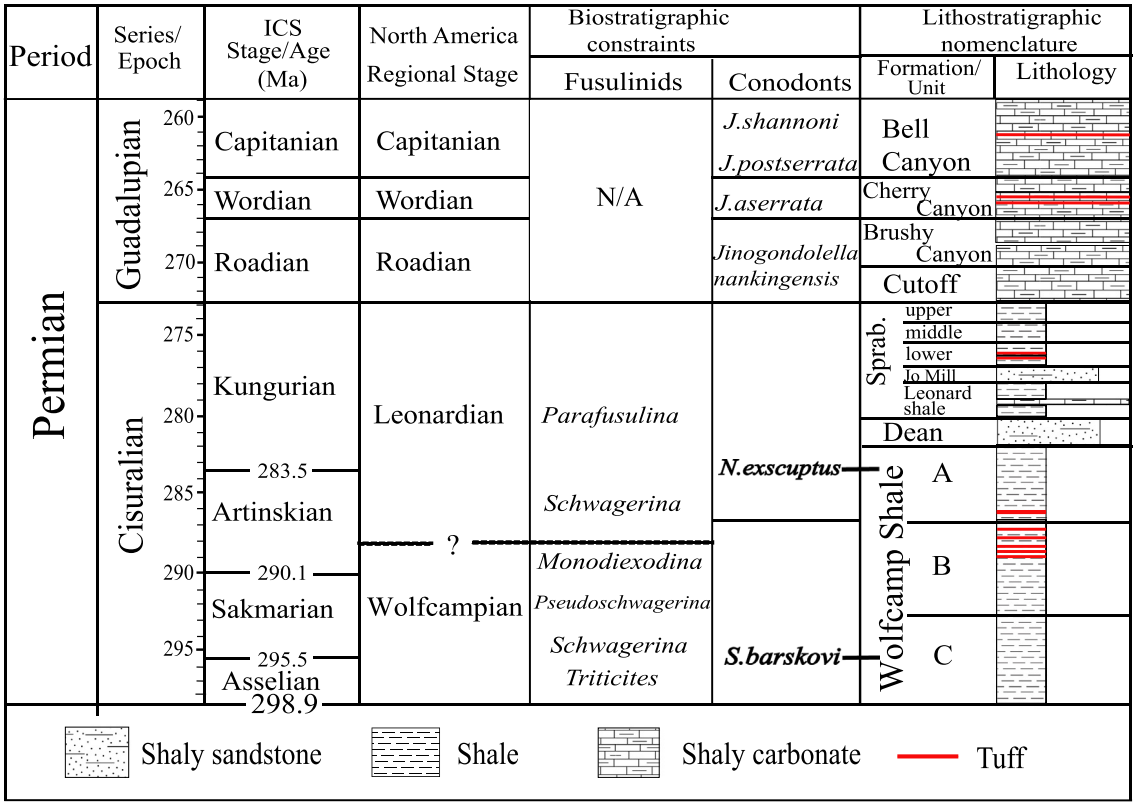

Fig. 2. Lower Permian stratigraphy in the Midland Basin and its correlation with the International Time Scale (International Commission of Stratigraphy, 2020). The lithostratigraphy and conodont zones of the Guadalupian Series are modified after Wu et al., (2019). The lithostratigraphic column of the Permian Series are modified after Heckel and Clayton (2006) and Henderson et al. (2012). Note that *S. barskovi* and *N. exscuptus* are conodonts that used to define the boundary between the Asselian Stage and Sakmarian Stage, and the Artinskian Stage and Kungurian Stage, respectively. Kohn et al. (2019) reported *S. barskovi* and *N. exscuptus* in the Wolfcamp A and Wolfcamp C units in northern Midland Basin.

et al. (2019) studied conodonts from core samples in the northern Midland Basin and proposed that the upper boundary of the Wolfcampian stage should be placed in the uppermost Wolfcamp B unit and the bases of the International Asselian, Sakmarian and Kungurian Stages should be placed in the lowermost Wolfcamp C, Wolfcamp C and Wolfcamp A units, respectively (Fig. 2). Leonardian stage in the Midland Basin contains the Dean and Spraberry Formations. The Dean Formation is mainly sandstone, and the Spraberry Formation consists of calcareous and silica-rich mudstone interbedded with siltstone and sandstone. The Spraberry Formation is further divided by oil industry geologists into several informal units, including the Leonard shale, Jo Mill sand, and lower, middle, and upper Spraberry (Handford, 1981; Hamlin and Baumgardner, 2012).

Three volcanic tuffs were collected from Guadalupian exposures in the Guadalupe Mountains, which is located on the northwestern margin of the Delaware Basin (Fig. 1) and is the site of GSSPs of the Guadalupian Roadian, Wordian and Capitanian epochs in ascending order (e.g., Glenister et al., 1992, 1999; Lucas and Shen, 2018). The Guadalupian Series consists of the Cutoff Formation, Cherry Canyon Formation, and the Bell Canyon Formation in ascending order (Fig. 2). The formations are dominated by siliciclastic rocks with some typical shelf carbonate facies proximal to shelf margins (Adams, 1965).

3. Materials and methods

3.1. Samples

Nine tuff horizons were identified from six Midland Basin subsurface cores (Fig. 1B) donated by Pioneer Natural Resources (*https://www.pxd.com*). These tuffs include six samples from the Wolfcamp B unit, one sample from the Wolfcamp A unit, and two samples from the Spraberry Formation (Figs. S1 and S2, Table S1 in the supplementary document). The six Wolfcamp B tuffs are from three cores and are correlated based on petrophysical data. One of the wolfcamp B tuffs is too thin and did not yield zircons. Five of the Wolfcamp B samples have insufficient grains of Permian age for statistical analysis, thus were combined as the Wolfcamp B tuff and the data is mostly from the Wolfcamp B5 sample.

The stratigraphic intervals of the tuffs were determined by petrophysical correlations following Hamlin and Baumgardner (2012) and Baumgardner et al. (2016). The base of the Wolfcamp A unit is characterized by an abrupt increase of gamma-ray signal referred as the "hot shale" marker, the base of the Wolfcamp B unit is marked by the middle Wolfcampian unconformity, the lower Wolfcamp C is marked by relatively low resistivity, and the Wolfcamp D unit has high gamma and high resistivity (Baumgardner et al., 2016). Our Wolfcamp A tuff is located about 45 m above the "hot shale" marker and our Wolfcamp B tuffs are located 20–60 m below the "hot shale" marker. The two Spraberry tuffs (Spraberry 1 and Spraberry 2) were collected from the lower Spraberry unit above the Jo Mill sand.

Oil industry geologists commonly identify tuffs based on fluorescence under ultraviolet light. The tuffs are greenish gray and show bright orange to dark brown fluorescence, and the interbedded shales are dark grey and do not show fluorescence (Fig. S2). Wolfcamp B tuffs are 3–12 cm thick, and the other tuffs are 2.5–5 cm thick. Some Wolfcamp B tuffs show erosional bases and wavy interbeds with shale (Fig. S2), suggesting erosion and transport. Tuffs in the other units show sharp lower and diffusive upper

boundaries indicating gradual settling without major perturbation during deposition. The physical appearance and major element compositions of these tuffs differ from those of the interbedded shales. The tuffs also contain abundant zircons and most zircons in this study are unrounded, unusual for deepwater shale. Although the abundance of detritus in these tuffs cannot be determined, following the definition that tuffs contain greater than 75% ash (Schmid, 1981), it is appropriate to classify the Wolfcamp A and Spraberry samples we studied as tuffs. The Wolfcamp B samples are most likely reworked tuffs (see our discussion).

Three tuff samples were collected from the Bell Canyon and Cherry Canyon Formations in the Guadalupe Mountains, at the same locations as sample BR040915-1B (our G1), NippleHill-2 (our G2), and MC053117-3 (our G3; Fig. S1) in Wu et al. (2020) (Table S1 in the supplementary document). All three tuffs are less than 20 cm thick and have grayish green color. The morphology and geochemistry of these tuffs have been described by Nicklen et al. (2015), and their ages have been determined using zircon U-Pb geochronology by Ramezani and Bowring (2018) and Wu et al. (2020).

3.2. Bulk tuff geochemistry

Bulk tuff major and trace elements were analyzed in the Shimadzu Center for Environmental, Forensics, and Material Science at the University of Texas at Arlington. Representative shale samples from the Wolfcamp B, Wolfcamp A and Spraberry units were also analyzed for comparison. Major element compositions were determined by a Shimadzu XRF-1800 wavelength dispersive X-ray fluorescence spectrometer. Trace element compositions were measured using a Shimadzu ICPMS2030 inductively coupled plasma mass spectrometer. See supplementary document under the section "Analytical Methods" for details.

3.3. Zircon morphology and geochemistry

Zircons were extracted from eleven tuff beds following standard procedures, including disc mill crushing, ultrasonic shaking to remove attached clays, pan washing, magnetic separation, and heavy liquid separation. All zircons from the tuffs were handpicked using a binocular microscope. Before mounting zircon grains in epoxy resin discs, a portion of the Wolfcamp A, Wolfcamp B, and Spraberry grains were randomly selected and imaged using a Hitachi S3000N scanning electronic microscope (SEM) to characterize grain morphology. These grains were classified into five classes of roundness following Gärtner et al. (2013). The classes include completely unrounded, poorly rounded, rounded, well rounded, and completely rounded following our study of the Mississippian Barnett tuff in the Permian Basin (Fig. S4 in Tian et al., 2022). After mounting and polishing, representative grains were imaged using a SEM and cathodoluminescence (CL) to observe internal zoning structures and inclusions to determine spots for U-Pb dating, Hf isotope analysis and rare earth element composition. Zircon grains primarily with volcanic textures such as muted, broad zonation under cathodoluminescence and morphologies with elongate tips, longitudinal gas tracks and transverse channels were primarily targeted for Laser Ablation-Inductively Coupled Plasma Mass Spectrometry (LA-ICPMS) and Chemical Abrasion-Isotope Dilution-Thermal Ionization Mass Spectrometry (CA-ID-TIMS) analyses. All zircon U-Pb dates, Lu-Hf isotope and trace element (TE) composition analysis by LA-ICP-MS were conducted at the Radiogenic Isotope and Geochronology Lab at Washington State University. After LA-ICPMS analyses, representative young zircon grains from Wolfcamp and Spraberry tuffs were plucked from the mount and analyzed at University of Wyoming by chemical abrasion, isotope dilution, thermal ionization mass spectrometry (CA-ID-TIMS) following Mattinson (2005). Analytical procedures, data reduction and filtering are described in the supplementary document under the section "Analytical Methods". For LA-ICPMS results, $^{207}Pb/^{206}Pb$ dates were used for grains older than 1300 Ma and $^{206}Pb/^{238}U$ dates were used for grains younger than 1300 Ma. Filters of 15% discordance (calculated as the ratio of $^{206}Pb/^{238}U$ and $^{207}Pb/^{206}Pb$ dates) and a 5% reverse discordance were applied to zircons older than 500 Ma to exclude grains that may have been influenced by Pb loss or poor matrix match between samples and standards leading to differential laser induced elemental fractionation (Allen and Campbell, 2012; Schaltegger et al., 2015). Discordance could not be used as a filter for grains less than 500 Ma because young ICPMS dates have large ^{207}Pb /^{206}Pb uncertainties, and many analyses appear to be -concordant.

4. Results

4.1. Whole rock geochemistry for Midland Basin tuffs

All tuff whole-rock samples had a loss on ignition (LOI) > 10%. After LOI normalization, the samples contain 59 to 70 wt% SiO_2, 21 to 31 wt% Al_2O_3, 0.3 to 0.5 wt% TiO_2, 2.2 to 3.9 wt% Fe_2O_3, 1.1 to 2.4 wt% MgO, 0.6 to 1.9 wt% CaO, 0 to 1.2 wt% P_2O_5 and 4.5 to 6.6 wt% $K_2O + Na_2O$ (Tables S2 and S3). On a K_2O-SiO_2 diagram, Spraberry tuffs plot as shoshonitic series and Wolfcamp tuffs plot as high-K calc-alkaline series (Fig. 3). In general, the tuffs show high Si, Al, and alkalis but low Ti content. Chemical index of alteration (CIA) of the samples was calculated using $Al_2O_3/(Al_2O_3 + CaO + K_2O + Na_2O)$. The CIA index of the tuff samples are between 0.73 and 0.82, higher than that of the shale samples (0.61–0.69).

On a Zr/TiO_2-Nb/Y diagram following Winchester and Floyd (1977), whole-rock trace element data place the tuffs into the dacite or andesite category (Fig. 4A). The tuffs are strongly enriched in large ion lithophile elements (LILE), such as Cs, Rb and Ba, and depleted in high field strength elements (HFSE), such as Nb, P and Ti (Fig. 4B). The samples plot in volcanic arc granite or within-plate granite settings in a Rb/(Y + Nb) plot (Pearce et al., 1984) (Fig. 4C). Chondrite-normalized rare earth element (REE) patterns are enriched in light REEs, show flat to slightly positive heavy REE slopes and moderate to no negative Eu anomalies with Eu/Eu* between 0.33 and 1.04 (Fig. 4D). All these features are typical of upper continental crust (Rudnick and Gao, 2003).

The shale samples have LOI from 7.4 to 21.7 %. After LOI normalization, the shale samples contain 55 to 75 wt% SiO_2, 5 to 16 wt%

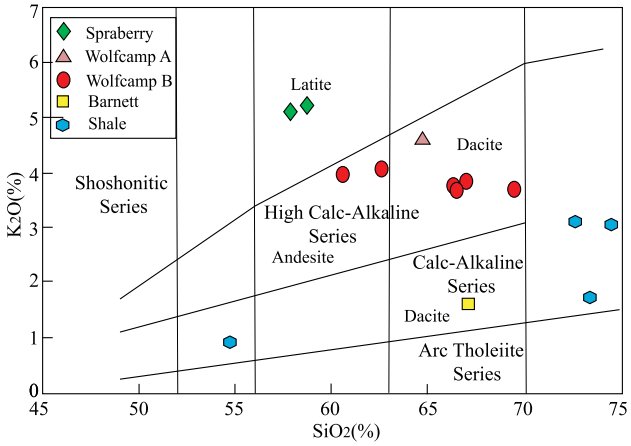

Fig. 3. K_2O vs. SiO_2 classification diagram showing whole rock major element compositions of the volcanic tuffs and shale, modified from Peccerillo and Taylor (1976).

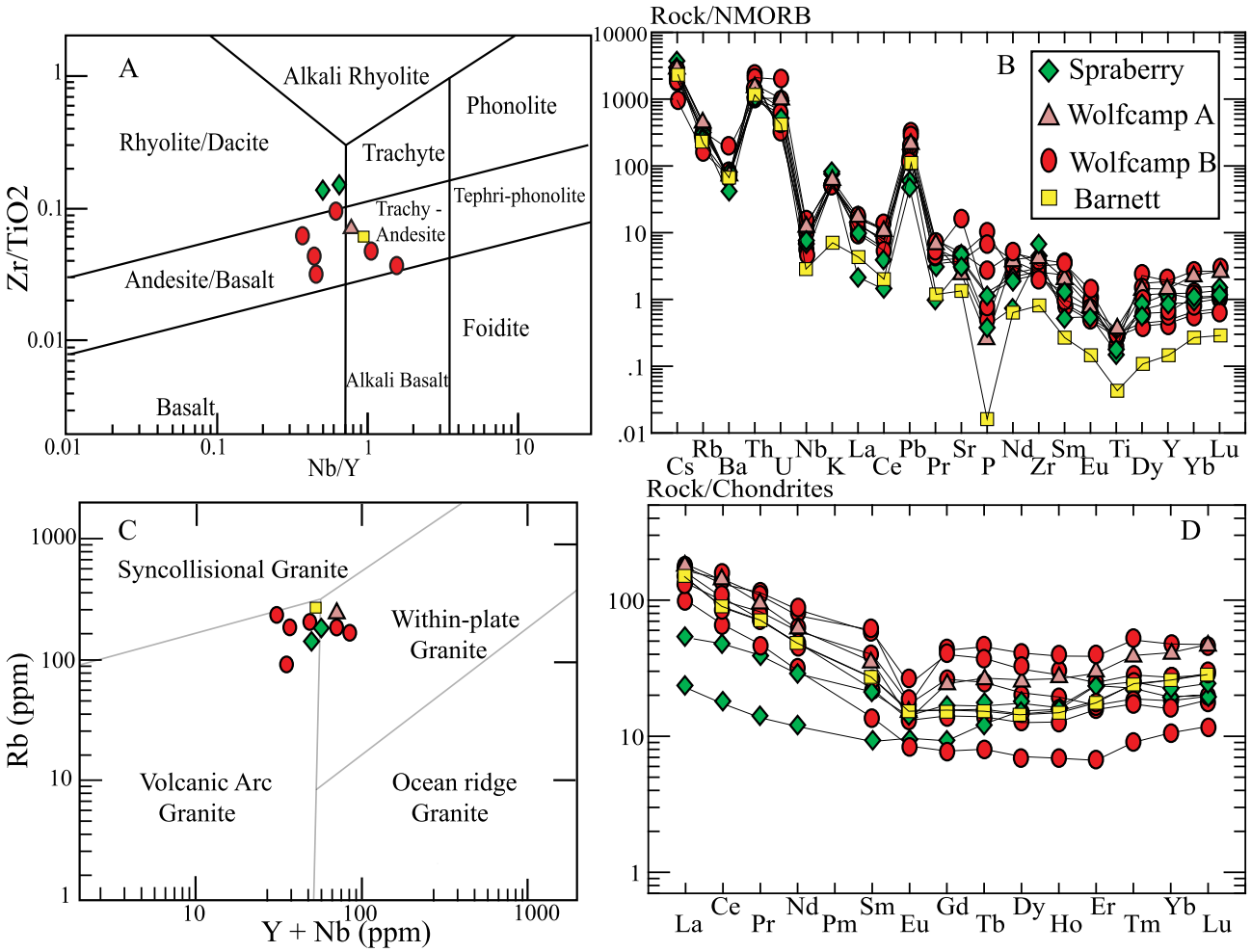

Fig. 4. Whole rock trace element diagrams of all the volcanic tuffs. A) Zr/TiO_2 vs. Nb/Y discrimination diagram, modified from Winchester and Floyd (1977). B) Mid-Ocean Ridge Basalt-normalized incompatible element diagram after Sun and McDonough (1989). C) Rb vs. Y + Nb discrimination diagram after Pearce et al. (1984). D) Chondrite-normalized REE diagram after Sun and McDonough (1989).

Al_2O_3, 0.1 to 0.8 wt% TiO_2, 2.27 to 4.3 wt% Fe_2O_3, 1.2 to 2.1 wt% MgO, 0.6 to 32.8 wt% CaO, 0 to 0.5 wt% P_2O_5 and 1.6 to 4.5 wt% $K_2O + Na_2O$ (Table S3). Wolfcamp A and Wolfcamp B are carbonate-rich and have high LOI and CaO values. In general, the shale samples have higher SiO_2, much higher CaO and much lower Al_2O_3 than the tuffs.

4.2. Zircon morphology and geochronology

Zircon roundness data show that about 73% of Wolfcamp B grains are rounded to completely rounded, while the percentage of roundness for the Wolfcamp A and lower Spraberry grains are 28% and 0%, respectively (Fig. 5). In addition, around 60% of the Wolfcamp B grains, but less than 30% grains from other units show fractures or collision marks.

After filtering, a total of 658 zircon LA-ICPMS U-Pb dates are reported in this study, including 460 for Midland Basin tuffs and 198 for Guadalupian tuffs (Fig. 6). Twenty-Eight dates are > 25 Ma younger than biostratigraphic ages and our CA-ID-TIMS dates, likely caused by lead loss or matrix mismatch between zircon reference and unknowns (Allen and Campbell, 2012; Schoene, 2014; Schaltegger et al., 2015; Coutts et al., 2019), and were excluded for age determination. A total of 29 CA-ID-TIMS dates are reported for Midland Basin tuffs. The depositional age of each tuff is interpreted as the weighted mean of the youngest CA-ID-TIMS dates (WMTIMS) (Fig. 7). The distribution of the LA-ICPMS dates for each sample is shown by kernel density estimation (KDE) (Fig. 8). The LA-ICPMS dates were interpreted using different statistical methods and the results were compared with the WMTIMS dates to determine the most appropriate method for interpreting LA-ICPMS dates (Fig. 8). Statistical methods include the youngest single grain date (YSG; Dickinson and Gehrels, 2009), weighted mean date of the youngest cluster of three or more grains overlap at 2σ error (YSP-youngest statistical population) with a mean square weighted deviation (MSWD) near 1 (Coutts et al., 2019), youngest mode date from the KDE (YMKDE) plot (cf. YPP of Dickinson and Gehrels, 2009), and TuffZirc date (TZ) on the youngest age group. TuffZirc uses a Monte Carlo model to generate a statistical youngest age from a group of genetically related grains (Ludwig and Mundil, 2002; Ludwig, 2008). A new statistical approach, weighted mean date of the youngest dominant KDE mode (WMYDM, Tian et al., 2022) with a MSWD near 1, is also used here for comparison. This method modifies the YSP approach from Coutts et al. (2019). We note that the dataset for YSP is much larger in Coutts et al. (2019) than in this study, but our dataset still permits useful comparisons between calculated dates. The youngest dominant population, which is the YSP, is assumed to be from a single eruptive event for volcanic tuffs. We use the KDE method described in Vermeesch (2012), which uses adaptative kernel density estimates. Adaptive kernel density

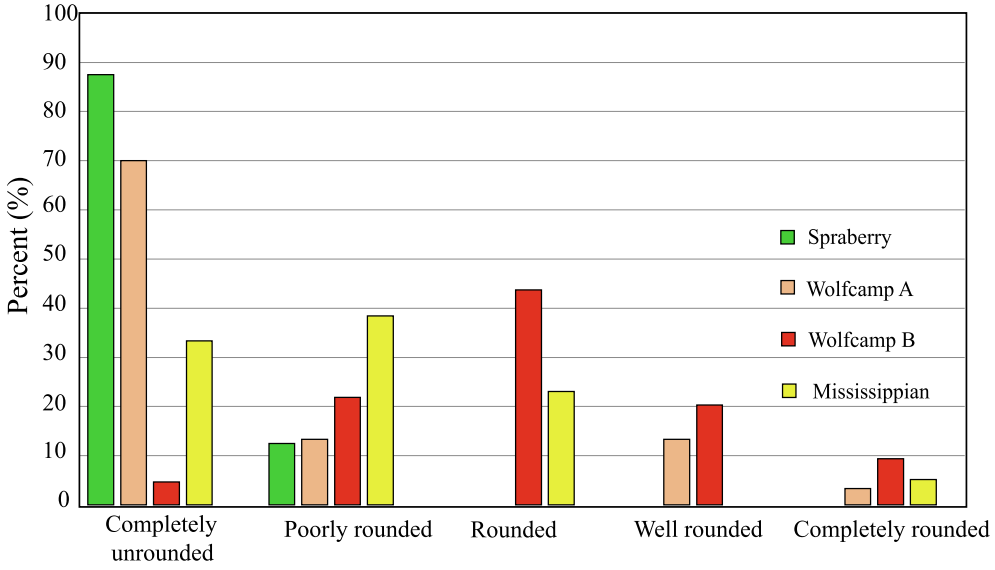

Fig. 5. Counts for each zircon roundness category for the Midland Basin tuffs. Pictures of different zircon morphology of the Mississippian Barnett tuff are published in Tian et al. (2022).

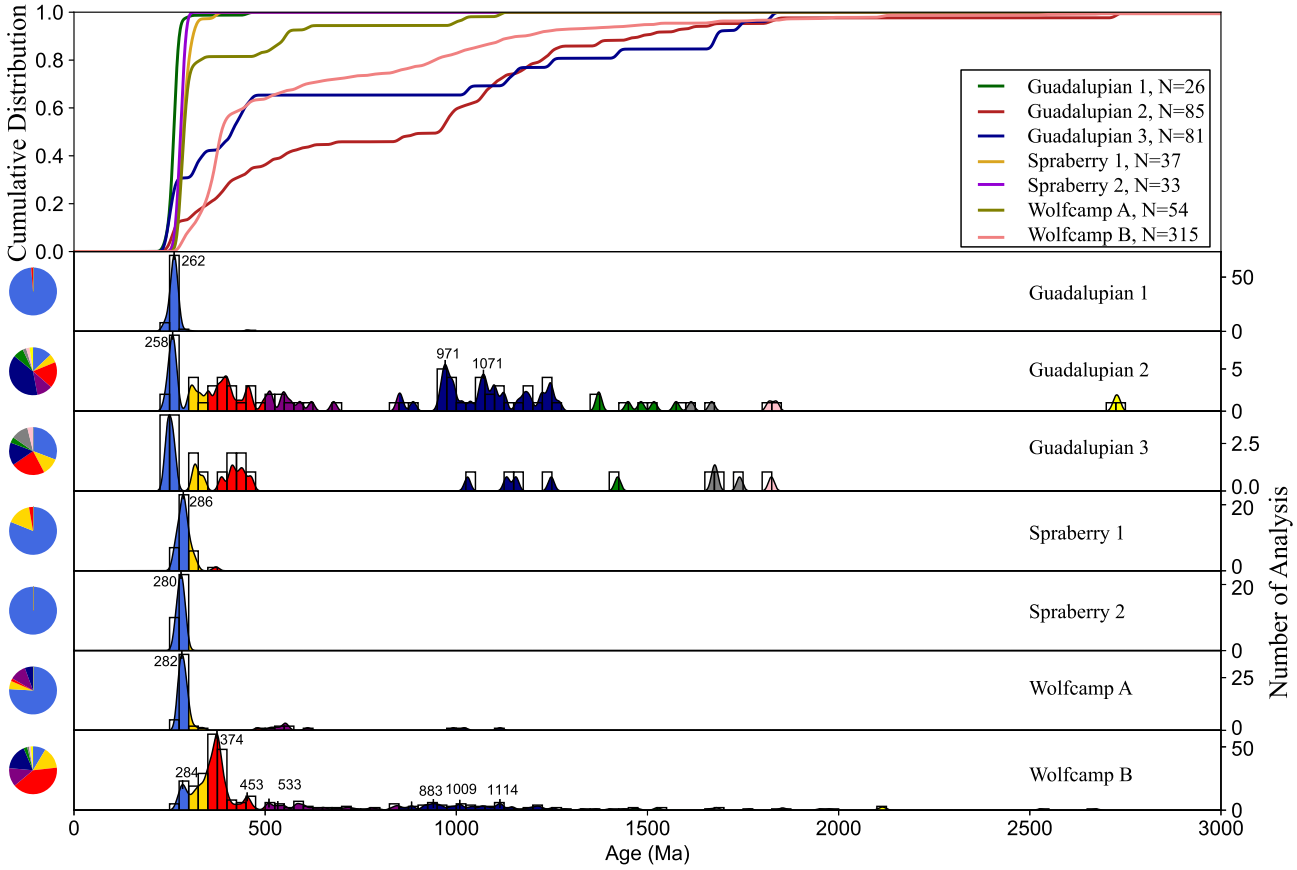

Fig. 6. Zircon LA-ICPMS U-Pb date distribution for all the volcanic tuffs. The plot is shown as kernel density estimation. The numbers on the plot are peak modes.

estimates vary the bandwidth according to the local density, which means that where data density is sparse, a large bandwidth is used, and the density estimate is smooth. To remove the influence of mode skewness, dates along both sides of the mode date are included progressively to derive a date with MSWD near 1. The WMYDM method excludes ICPMS dates at both tails of the distribution that do not overlap at 2σ with the mode. These scattered dates typically reflect Pb loss, matrix effect-related bias, and inheritance of grains from the magma source (e.g., Schaltegger et al., 2015). The youngest mode date from the PDP plot of each tuff is also calculated, but not reported here as PDP oversmooths date distribution of all our samples (see details in discussion).

A total of 114 zircon Hf isotopic values were analyzed with 24 for the middle Permian G3 tuff, 16 for the Spraberry 1 tuff, 10 for

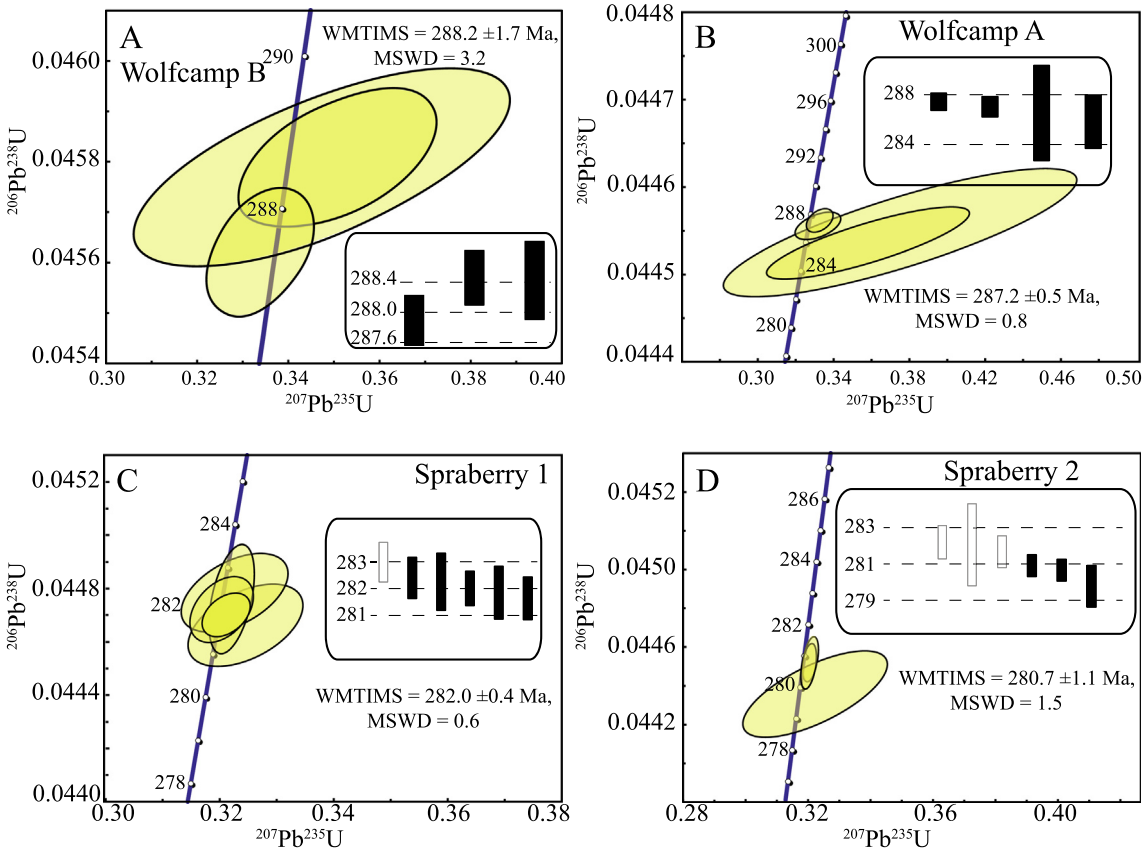

Fig. 7. Concordia plots ($^{206}Pb/^{238}U$ vs. $^{207}Pb/^{235}U$) and weighted mean of the CA-ID-TIMS dates for the Wolfcamp B (A), Wolfcamp A (B), Spraberry 1(C) and Spraberry 2 (D) tuffs. Zircon dates marked by black bars are used to calculate the true depositional ages. The reported CA-ID-TIMS uncertainties are 2σ.

the Spraberry 2 tuff, 26 for the Wolfcamp A tuff, and 38 for the Wolfcamp B tuff. Most Hf analyses were conducted on grains with dates close to their CA-ID-TIMS dates.

4.2.1. Wolfcamp B tuff

A total of 314 LA-ICPMS and 7 CA-ID-TIMS zircon U-Pb dates were interpreted for the Wolfcamp B tuff. LA-ICPMS dates range from 2673 ± 39 to 270 ± 7 Ma (YSG) with 9% < 300 Ma, 58% between 300–500 Ma, 11% between 500–850 Ma, 15% between 900–1300 Ma, 5% between 1300–2000 Ma, and 2% > 2000 Ma (Fig. 6). The WMTIMS was calculated to be 288.2 ± 1.7 Ma from three of the young CA-ID-TIMS dates (Fig. 7A). Although the tuff is most likely reworked and the date is potentially a maximum age, this date is the true depositional age (TDA) for it cannot be younger than the Wolfcamp A tuff at a higher stratigraphic level. A total of 27 LA-ICPMS dates ranging from 277.3 ± 3.4 to 306.6 ± 1 3.6 Ma were used for statistical calculations (Fig. 8). The YMKDE date is 286 Ma, the WMYDM date calculated from 7 dates is 288. 6 ± 1.5 Ma (MSWD = 1.1), the YSP date calculated from 4 grains is 278.3 ± 1.7 Ma (MSWD = 1.1), and the TZ date calculated from 12 grains is 283.5 + 2.1/−1.3 Ma.

Hf isotope analysis of Wolfcamp B zircons was conducted on both the < 300 Ma cluster representing the volcanic zircons, and > 300 Ma zircons interpreted as being detrital or inherited from the upper crustal source. All large grains in the volcanic group were analyzed for Hf isotopes, yielding seven analyses. The seven grains, with LA-ICPMS dates between 284.7 ± 3.3 Ma and 291.3 ± 4.7 Ma, have εHf values between +0.5 and +8.8 with an average of +5.5. A total of 29 Hf data points are from detrital/inherited grains. In the 300–500 Ma group, 24 grains, with LA-ICPMS dates ranging from 345.3 ± 3.7 Ma to 465.8 ± 15.1 Ma, have εHf values between −5.2 and +6.3 with an average of +2.8. Only two grains have negative Hf values. In the 500–850 Ma group, four grains, with LA-ICPMS dates between 525 ± 19 Ma and 639.2 ± 8.9 Ma, have εHf values ranging from −2.7 to +12.7 with an average of +7.2. The T_{DM2} age ranges from 675 Ma to 1207 Ma for volcanic grains and from 550 to 1652 Ma for detrital grains.

4.2.2. Wolfcamp A tuff

A total of 54 LA-ICPMS and six CA-ID-TIMS zircon U-Pb dates were measured from the Wolfcamp A tuff. LA-ICPMS dates range from 1114 ± 16 to 273.4 ± 6.2 Ma (YSG) with 76% < 300 Ma, 7% between 300–500 Ma, 11% between 500–850 Ma, and 6% between 900–1300 Ma (Fig. 6). The WMTIMS is 287.2 ± 0.5 Ma based on the four youngest CA-ID-TIMS dates (Fig. 7B). A total of 41 LA-ICPMS dates ranging from 273.4 ± 6.2 to 317.4 ± 5.6 Ma were used for statistical calculations (Fig. 8). The YMKDE is 282 Ma, the WMYDM date calculated from 10 dates is 288.1 ± 1.1 Ma (MSWD = 1), the YSP date calculated from 14 dates is 276.0 ± 1.0 Ma (MSWD = 1.1), and the TZ date calculated from 17 dates is 278.2 + 1.6/−2.5 Ma.

Among the 26 Wolfcamp A Hf analyses, 19 grains with LA-ICPMS dates ranging from 280.9 ± 3.5 Ma to 298.6 ± 3.6 Ma show εHf values varying from −2.2 to −6.0 with an average of −4.5. The T_{DM2} ages of all grains are between 1381 and 1616 Ma.

4.2.3. Spraberry tuffs

A total of 37 LA-ICPMS and 8 CA-ID-TIMS U-Pb dates were interpreted for the Spraberry 1 tuff. LA-ICPMS dates range from 371.2 ± 13.9 to 262.7 ± 9.7 Ma (YSG) with 81% <300 Ma and 19% between 300 and 500 Ma (Fig. 6). The WMTIMS was calculated to be 282.0 ± 0.4 Ma from the youngest five dates (Fig. 7C). A total of 31 Spraberry dates ranging from 262.7 ± 9.7 Ma to 300.9 ± 9.5

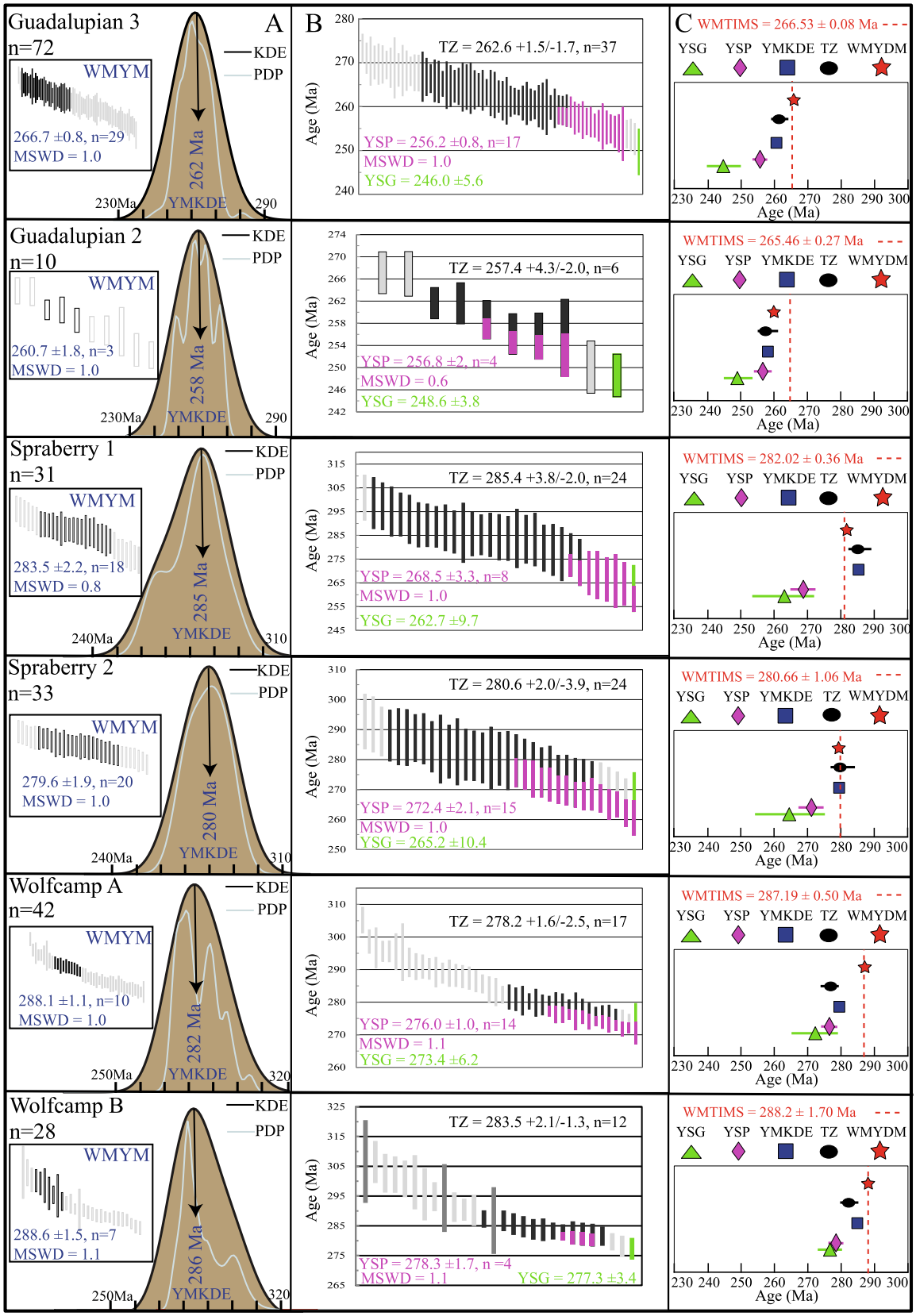

Fig. 8. Comparison of statistical LA-ICPMS dates and the true depositional ages determined by CA-ID-TIMS dating. Column A is the distribution of the youngest peak mode with both probability density plot (PDP) and kernel density estimation (KDE). Zircon dates marked in black lines are used for the mode. Column B is the age distribution and statistical results of the youngest single grain date (YSG, dates marked in green color), weighted mean of the youngest cluster date (YSP, dates marked in purple color) and TuffZirc date (TZ, dates marked in black color). MSWD (mean square weighted deviation), weighted mean age of the youngest dominant KDE mode (WMYDM) with MSWD near 1 is the preferred statistical LA-ICPMS date. Column C compares weighted mean CA-ID-TIMS dates (WMTIMS) with calculated dates from LA-ICPMS data alone. (For interpretation of the references to color in this figure legend, the reader is referred to the web version of this article.)

Ma were used for statistical calculations (Fig. 8). The YMKDE is 285 Ma, the WMYDM calculated from 18 dates is 283.5 ± 2.2 Ma (MSWD = 0.8), the YSP calculated from 8 dates is 268.5 ± 3.3 Ma (MSWD = 1.0), and the TZ date calculated from 24 dates is 285.4 + 3.8/−2.1 Ma.

A total of 33 LA-ICPMS and 8 CA-ID-TIMS U-Pb dates were interpreted for the Spraberry 2 tuff. The LA-ICPMS dates range from 292.7 ± 9.1 to 265.2 ± 10.4 Ma (YSG) (Fig. 6). The WMTIMS was calculated to be 280.7 ± 1.1 Ma from the three youngest dates (Fig. 7D). All LA-ICPMS dates were used for statistical calculations (Fig. 8). The YMKDE is 280 Ma, the WMYDM date calculated from 20 dates is 279.6 ± 1.9 Ma (MSWD = 1), the YSP date calculated from 15 dates is 272.4 ± 2.1 Ma (MSWD = 1.0), and the TZ calculated from 24 dates is 280.6 + 2.1/−3.9 Ma.

Among the 16 Spraberry 1 Hf analyses, 9 zircons with LA-ICPMS dates between 272.9 ± 5.6 and 288.0 ± 8.6 Ma are considered volcanic, and these have εHf values between +0.5 and −6.0 with an average of −2.3. Among the 10 Spraberry 2 Hf analyses, 9 zircons with LA-ICPMS dates between 271.2 ± 8.1 and 297.9 ± 9.1 Ma are considered volcanic and their εHf values range from −0.4 to −5.1 with an average of −3.5. The T_{DM2} ages of all Spraberry zircons are between 1197 and 1649 Ma.

4.2.4. Guadalupe Mountains tuffs

A total of 26 LA-ICPMS zircon U-Pb dates were obtained for the G1 tuff. A CA-ID-TIMS date of 262.1 ± 0.1 Ma was reported by Wu et al. (2020) for this tuff. The LA-ICPMS dates range from 1824 ± 49 to 241.6 ± 3.1 Ma (YSG) with 31% <270 Ma, 35% between 300–500 Ma, 8% between 900–1300 Ma, and 27% between 1300–2000 Ma (Fig. 6). The available young dates are not sufficient to generate PDP or KDE plots or calculate a TZ date. The YSP was calculated to be 260.4 ± 6.7 Ma (MSWD = 2.6) from three dates.

A total of 85 LA-ICPMS zircon U-Pb dates were obtained for the G2 sample. A CA-ID-TIMS date of 265.5 ± 0.3 Ma was reported by Wu et al. (2020). The LA-ICPMS dates range from 2732 ± 20 to 240.0 ± 3.0 Ma (YSG) with 13% < 300 Ma, 24% between 300–500 Ma, 12% between 500–850 Ma, 36% between 900–1300 Ma, 13% between 1300–2000 Ma, and 2% > 2000 Ma (Fig. 6). A total of 10 LA-ICPMS dates ranging from 246.8 ± 3.8 to 267.1 ± 3.8 Ma (YSG) were used for statistical calculations (Fig. 8). The YMKDE is 258 Ma, the WMYDM calculated from three dates is 260.7 ± 1.8 Ma (MSWD = 1.0), the YSP calculated from four dates is 256.8 ± 2.0 Ma (MSWD = 0.6), and the TZ calculated from six dates is 257.4 + 4.3/−2.0 Ma.

A total of 81 LA-ICPMS zircon U-Pb dates were reported for the G3 sample. A CA-ID-TIMS date of 266.5 ± 0.1 Ma was reported by Wu et al. (2020). The LA-ICPMS dates range from 1824 ± 49 to 235.5 ± 5.6 Ma (YSG) with 98% < 300 Ma and 2% > 300 Ma (Fig. 6). Seventy-three LA-ICPMS dates ranging from 246.0 ± 5.6 M a to 281.4 ± 4.9 Ma were used for statistical calculations (Fig. 8). The YMKDE is 262 Ma, the WMYDM calculated from 29 dates is 266.7 ± 0.8 Ma (MSWD = 1.0), the YSP calculated from 17 grains is 256.2 ± 0.8 Ma (MSWD = 1), and the TZ calculated from 37 dates is 262.6 + 1.5/−1.6 Ma. The εHf values of 24 grains with LA-ICPMS dates between 263.1 ± 5.2 and 270.3 ± 5.5 Ma range from +1.9 to −2.8 with an average of −0.1. The T_{DM2} of all the grains are between 1102 and 1401 Ma.

4.2.5. Mississippian tuffs

As a comparison, data reported for the Mississippian Barnett tuff in the Midland Basin and five Mississippian tuffs in the Stanley Group in the Ouachita Mountains (Tian et al., 2022) are summarized here. The Barnett tuff in the Midland Basin has LA-ICPMS zircon dates from 339.9 ± 4.3 Ma to 300.4 ± 4.4 Ma (YSP), a WMTIMS of 327.8 ± 0.8 Ma, YSP of 304.0 ± 1.2 Ma, YMKDE of 325 Ma, WMYDM of 326.7 ± 0.6 Ma, and TZ of 326.2 + 1.0/−0.6 Ma. Zircons between 340 and 308 Ma have ε_{Hf} values mostly between 0 and +5 with an average of +2. The T_{DM2} ranges between 682 and 1432 Ma.

4.2.6. Summary

Nearly all statistical approaches for interpreting LA-ICPMS data yield U-Pb dates somewhat younger than the corresponding WMTIMS dates in this study (Fig. 8C). The YSPs are 10 to 20 Myr younger than the corresponding WMTIMS dates, but the other statistical treatments of LA-ICPMS ages are within 96% of the WMTIMS dates. Among the statistical approaches, the WMYDM best approximates WMTIMS dates despite the fact that the Wolfcamp A and Wolfcamp B distributions are skewed toward younger dates and the Spraberry 1 distribution is slightly negatively skewed toward old dates (Fig. 8A).

Hf isotopes distinguishes older and younger tuffs. Mississippian tuffs (average εHf = +2) and Wolfcamp B tuffs (average εHf = + 5.5) have younger T_{DM2} model ages (675 and 1432 Ma). The Wolfcamp A and Spraberry tuffs have an average εHf < −2.2 and older T_{DM2} model ages (1197–1649 Ma). The middle Permian G3 tuff shows an intermediate Hf signature with an average ε_{Hf} close to 0 and T_{DM2} model ages between 1102 and 1401 Ma.

4.3. Zircon trace element (TE) compositions

A total of 58 zircon TE compositions were analyzed: 30 for the G1 tuff, 13 for the Wolfcamp A tuff and 15 for the Wolfcamp B tuff. Zircons from all units show high ∑REE, enrichment of HREEs, negative Eu anomalies (average = 0.4) and positive Ce anomalies (average = 19.7) (Fig. 9A). Discrimination diagrams following Belousova et al. (2002) and Grimes et al. (2015) project these tuffs to the granitoid parent magma composition and continental arc setting (Fig. 9B, 9C).

5. Discussion

Below we use our new data to discuss four topics: 1) how well do LA-ICPMS and CA-ID-TIMS U-Pb zircon ages agree; 2) the implications for Permian Basin chronostratigraphy; 3) where was the volcano(es) that ejected the ashes? and 4) the implications for understanding the late Paleozoic tectonic evolution of southern Laurentia.

5.1. Comparison of LA-ICPMS and CA-ID-TIMS dates

Constraining TDA of tuffs from zircon U-Pb dates is limited by analytical precision and by potential inaccuracies introduced by Pb loss and matrix mismatches from LA-ICPMS methods. LA-ICPMS is the most used zircon U-Pb dating technique given its low cost and rapid data acquisition, but has low analytical precision (>1%; Gehrels, 2014). Systematic offsets by laser ablation, likely reflecting matrix effects caused by mismatch of standards and unknowns, are commonly observed (Allen and Campbell, 2012; Schoene, 2014; Schaltegger et al., 2015; Coutts et al., 2019). These uncertainties do not affect CA-ID-TIMS dates, which have typical analytical precisions of ~0.1% (Gehrels, 2014). Results derived from statistical treatment of LA-ICPMS dates are frequently used to approximate TDA, but all these statistical approaches could be biased by lead loss, statistical defects, and matrix effects, and the influence of each of these three factors on statistical dates is variable (Coutts et al., 2019). Our dataset adds to the few studies that identify the best statistical approaches for interpretating LA-ICPMS dates to match CA-ID-TIMS dates (e.g., Spencer et al., 2016; Herriott et al., 2019).

In this study, the WMTIMS date is taken as the TDA for each tuff and is compared with other LA-ICPMS statistical dates. All the YSGs

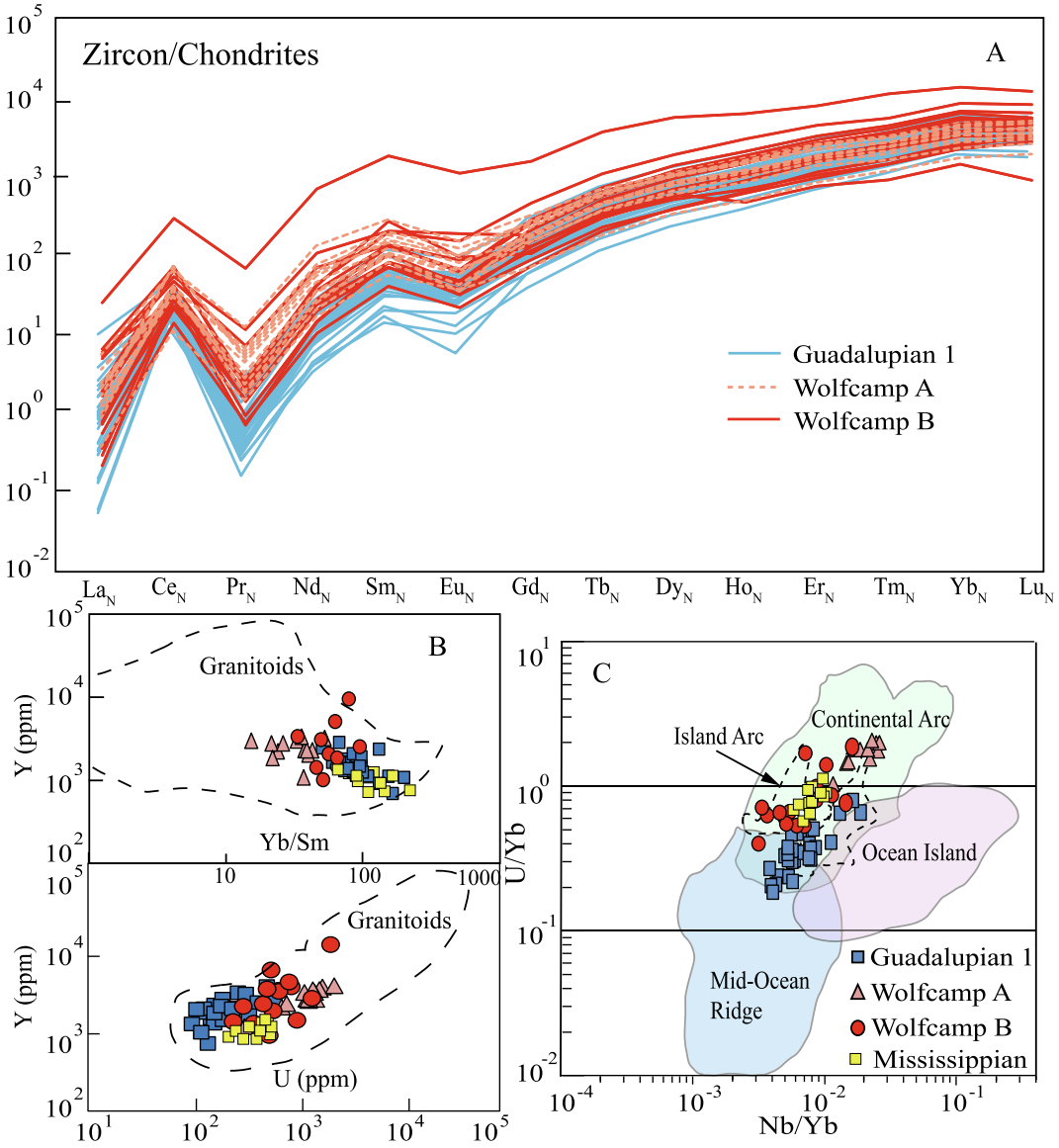

Fig. 9. A) Zircon rare earth element compositions normalized to chondrites following McDonough and Sun (1995). B) Zircon trace element composition discrimination diagram following Belousova et al. (2002). C) Zircon trace element composition discrimination diagram following Grimes et al. (2015).

are 10–20 Myr younger than the TDAs which may be mainly attributed to lead loss (Coutts et al., 2019). Half of the grains dated by both LA-ICPMS and CA-ID-TIMS have LA-ICPMS dates older than WMTIMS dates (Fig.S3), which is most likely caused by matrix effect (Allen and Campbell, 2012) for the LA-ICPMS data or may reflect antecrystic, pre-eruptive or inherited zircons for the CA-ID-TIMS data. Although inheritance of older cores may cause LA-ICPMS dates older than TDAs, such grains have been excluded based on CL image screening before analysis. Our comparison further shows that nearly all the statistical dates from LA-ICPMS data are somewhat younger than the TDAs, agreeing with the results of previous studies (Coutts et al., 2019; Herriott et al., 2019). Because of the influence of lead loss, YSP and YC2σ (mean date of the youngest cluster at 2σ error, Dickinson and Gehrels, 2009) dates that selectively sample grains from the negative tail (young date) of the distribution will likely result in an erroneously younger interpreted TDA.

Our results also show that the YMKDE, TZ, and WMYDM dates (Fig. 8C) are within 96% of the TDAs although often biased toward younger dates, suggesting that all these dates can be used to approximate TDAs if CA-ID-TIMS dates are not available. Among these approaches, the WMYDM dates are consistently the closest to the TDA dates. This is different from the results of previous studies, which showed that the YSP dates best approximate detrital zircon maximum depositional ages because of their high coincidence with CA-ID-TIMS dates (Herriott et al., 2019). This difference with our results might reflect the fact that ours are dominantly *syn*-depositional volcanic zircons with a single mode from a single eruption (cf., Cawood et al., 2012; Spencer et al., 2016). The PDP distribution is widely used to display zircon dates and recognize modes (Ludwig, 2008). The PDP was designed to reduce the importance of imprecise measurements and emphasize more precise measurements by taking the individual analytical precision as the bandwidth, which, however, can produce noisy results when applied to high-precision data and yield oversmoothed density estimations when dataset is large and/or analytical precision is low (Vermeesch, 2012). The PDP overfits all of our LA-ICPMS analyses (Fig. 8A) because of low analytical precision. The KDE deploys the Gaussian distribution by adapting the bandwidth according to local density without considering individual analytical precision

(Vermeesch, 2012). The Wolfcamp A and Wolfcamp B LA-ICPMS age distributions are positively skewed (to young dates) and the Spraberry 1 distribution is negatively skewed (to old dates) (Fig. 8A), which result in younger and older YMKDE dates than the TDAs, respectively. The comparison shows that the skewness of LA-ICPMS dates should be carefully evaluated before the YMKDE approach is used. Our study confirms that WMYDM approach compensates for skewness by calculating the mean of the mode dates with MSWD near 1 and better approximates the TDAs.

If the accuracy of TDA needs to be better than ± 4% for a given application, our results suggest that it is important to pair LA-ICPMS data with CA-ID-TIMS analyses. Chemical abrasion removes the effects of Pb loss and isotope dilution minimizes the dependence on standard analyses for measuring dates thereby avoiding potential matrix-induced inaccuracies from LA-ICPMS derived TDAs (Schoene, 2014; Schaltegger et al., 2015). An alternative strategy of annealing zircons and standards prior to LA-ICPMS analysis has been championed by Allen and Campbell (2012) as it seems to minimize matrix effects and yield LA-ICPMS dates that are within 0.5% of CA-ID-TIMS dates. Merely annealing zircons prior to analysis would not require the sophisticated labs and methods needed for complete chemical abrasion and could be more widely applied.

5.2. Implications for Permian Basin chronostratigraphy

The development of the oil industry in the Permian Basin resulted in complicated lithostratigraphic nomenclature (e.g., Montgomery, 1996). The early Permian North American regional stages were mainly studied in the well-exposed Permian section in the Glass Mountains to the southwest of the Delaware Basin (e.g., Behnken, 1984; Wardlaw and Davydov, 2000; Ross and Ross, 2003; 2009; Wahlman, 2013; Wardlaw and Nestell, 2014). The subsurface stratigraphic architecture of the Midland Basin was primarily constrained by petrophysical log signatures referenced to the type sections in the Glass Mountains (e.g., Mazzullo and Reid, 1989; Hamlin and Baumgardner, 2012; Baumgardner et al., 2016). Ages presented in this study improves the chronostratigraphy.

Recent biostratigraphy studies in the Permian Basin suggest that the Pennsylvanian-Permian boundary is in the lowermost Wolfcamp C unit and that the Wolfcampian-Leonardian boundary should be placed in the uppermost Wolfcamp B unit (e.g., Wahlman et al., 2016; Kohn et al., 2019). These studies also suggest that the boundaries of the Asselian, Sakmarian, Artinskian and Kungurian stages are in the uppermost Wolfcamp C, middle Wolfcamp B, and Wolfcamp A units, respectively (Fig. 2). Assuming the Pioneer proprietary stratigraphic correlations are correct, our new dates have implications for the absolute ages of the Wolfcamp Shale. Our Wolfcamp A and Wolfcamp B tuffs have WMTIMS dates of 287.2 ± 0.5 Ma and 288.2 ± 1.7 Ma, respectively, consistent with biostratigraphy results that correlate the Wolfcamp B unit to the late Sakmarian and early Artinskian stages and the Wolfcamp A unit to the late Artinskian stage. Based on the stratigraphic thickness between the two tuffs (Pioneer proprietary information), assuming a stable sedimentation rate, the data yield an average sedimentation rate of ~65 m/Myr (0.065 mm/y) for the upper Wolfcamp B and lower Wolfcamp A unit. The base of the Wolfcamp C unit is about 396 m below the Wolfcamp B tuff. If the base of Wolfcamp C is considered the beginning of the Permian Period (298.9 Ma), the average sedimentation rate in the Wolfcamp C and lower Wolfcamp B unit is ~37 m/Myr (0.037 mm/y). Given these rocks have experienced compaction, the estimated sedimentation rates are higher than modern average global ocean pelagic sedimentation rate which is less than 35 m/Myr (0.035 mm/y) (e.g., Davies et al., 1977). The sedimentation rate almost doubled from the Wolfcamp C-lower Wolfcamp B unit to the upper Wolfcamp B-lower Wolfcamp A unit, which likely reflects an increase in turbidite sedimentation in the Wolfcamp B unit given turbidites are well documented in lower Permian strata in the Permian Basin (Hamlin and Baumgardner; 2012; Baumgardner et al., 2016).

The two Spraberry samples reside in the same lithostratigraphic interval based on well logs. Studies of fusulinid microfossils show that the Spraberry Formation is of Leonardian age (e.g., Silver and Todd, 1969; Handford, 1981). The two Spraberry tuffs have WMTIMS dates of 282.0 ± 0.4 and 280.7 ± 1.1 Ma, overlapping within uncertainty. The Spraberry tuffs are ~365 m above the Wolfcamp A tuff. If the mean WMTIMS date (281.4 Ma) of the two tuffs is used, the sedimentation rate between the upper Wolfcamp A unit and the lower Spraberry Formation is ~49 m /Myr (0.049 mm/y), lower than that of the upper Wolfcamp B-Wolfcamp A unit.

5.3. Magmatic affinity and source of the tuffs

Alteration of the late Paleozoic tuffs makes the whole rock geochemistry data less reliable. The whole rock major and trace element data show dacite or andesite compositions (Figs. 3 and 4) while zircon trace element data show granitic composition (Fig. 9), most likely because of diagenesis of the tuffs. It has been suggested that the formation of zeolites by altering volcanic glass in tuffs is accompanied by increases in Mg and Al contents and decrease in Si content (e.g., Marantos et al., 2008). Alteration of the bulk tuffs is further supported by the high CIA index. Alteration of tuffs also causes rare earth element fractionation (e.g., Murakami and Ishihara, 2008). Therefore, the whole rock geochemistry data are not used to interpret the source of the tuffs.

Our zircon trace element data suggest that all the tuffs came from continental arcs with granitoid parent magma compositions (Fig. 9). The εHf dropped from an average of +5.5 to −4.5 between the Wolfcamp B and Wolfcamp A volcanic zircons within 1 Myr. Zircon Hf signature of magmatic units that were adjacent to the Permian Basin during the late Paleozoic are plotted together with our data for discussing parent magma affinity and sources of different tuffs (Fig. 10).

5.3.1. Mississippian tuffs

Tian et al. (2022) compared the geochemical signature of Mississippian tuffs (328–317 Ma) in the Midland Basin and Ouachita Mountains with other magmatic units and suggested that these tuffs were most likely from a northern Gondwana arc. The study further suggested that the arc was developed on the Maya or Sabine block by southward subduction of the Rheic ocean beneath the *peri*-Gondwana realm in northern Gondwana (Fig. 1C). The T_{DM2} ages are between 682 and 1432 Ma, suggesting that the arc developed on crust with both Grenville and Pan-African affinities (Tian et al., 2022). The Aserradero Rhyolite near Ciudad Victoria, Mexico, has continental arc geochemical signature with zircon crystallization ages of 348–340 Ma (Ramírez-Fernández et al., 2021), suggesting that the northern Gondwana arc may have started as early as the Early Mississippian.

5.3.2. Wolfcamp B tuffs

Some Wolfcamp B tuffs were reworked because they have erosional contacts with the underlying shale and wavy bedding (Figs. S1 and S2). The tuffs have abundant old (>300 Ma) and rounded grains (Fig. 5), indicating that some or all of the tuffs were redeposited and/or mixed with detrital sediments. Nevertheless, there are sufficient angular, magmatic grains to obtain a WMTIMS age of 288.2 ± 1.7 Ma. Magmatic units of similar age and geochemical compositions include 1) plutonic rocks in the Honduras batholith of the Oaxacan and Acatlán metamorphic complexes

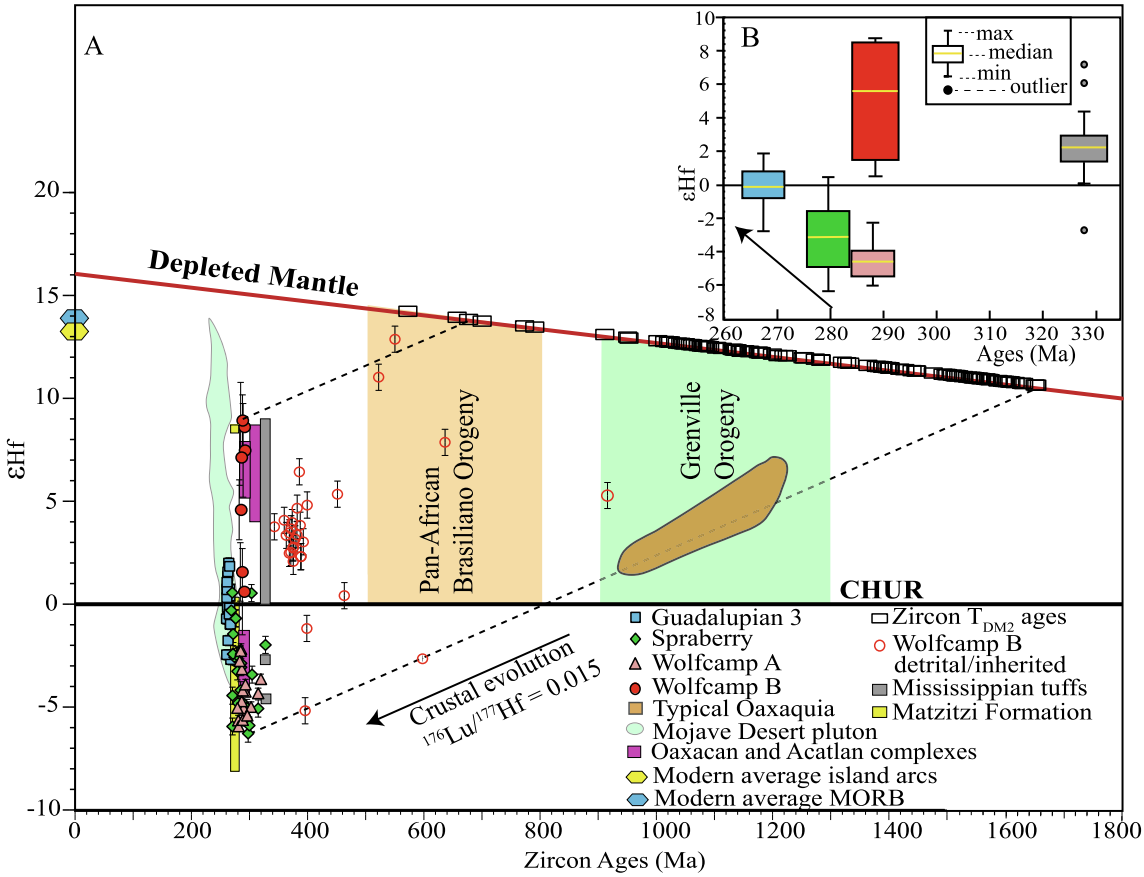

Fig. 10. A) Zircon U-Pb dates, ε_{Hf} values and T_{DM2} ages of the volcanic tuffs are compared with those of the Andean continental arc (Jones et al., 2015), average island arc (Dhuime et al., 2011), mid ocean ridge basalt (MORB, Workman and Hart, 2005), and Late Paleozoic magmatic rocks in the Ouachita-Marathon region and Mexico. T_{DM2} ages were calculated using an average crustal value of $^{176}Lu/^{177}Hf = 0.015$ following Griffin et al. (2002). Oaxacan and Acatlán complexes data are from Ortega-Obregón et al. (2014). Matzitizi Formation data are from Zúñiga et al. (2020). Mississippian tuff data are from Tian et al. (2022). Mojave Desert pluton data are from Cecil et al. (2019). "Typical Oaxaquia" data are from Weber et al. (2010). CHUR means chondritic uniform reservoir. Note that the ε_{Hf} values become more juvenile from the Wolfcamp A and Spraberry tuffs to Guadalupian tuffs and the trend is consistent with that in the Mojave Desert pluton data (Cecil et al., 2019). B) Box plot of zircon U-Pb dates, ε_{Hf} values of volcanic tuffs for the sample G3 (266.5 Ma), Spraberry (279.8 Ma), Wolfcamp A (287.2 Ma) and Wolfcamp B (288.2 Ma), the legends are the same with A. The ages of the tuffs in the box plot are the interpreted true depositional ages for these tuffs. The width of the box plot does not represent the uncertainty of the age.

(Oaxaquia terrane) in southern Mexico, which are tonalite to quartz diorite with a zircon LA-ICPMS date of 290 ± 2 Ma, ε_{Hf} values between +5 and +8, and T_{DM2} model ages between 795 and 948 Ma (Ortega-Obregón et al., 2014); 2) quartz diorites in the Totoltepec pluton of the Acatlán metamorphic complex, which has a zircon LA-ICPMS date of 289 ± 2 Ma, whole rock ε_{Nd} values between −0.8 and +2.6, and T_{DM} model ages between 930 and 1160 Ma (Kirsch et al., 2012); 3) granitoids with zircon LA-ICPMS dates of 294 ± 3 Ma in the Oaxaquia terrane on the western margin of Gulf of Mexico (Coombs et al., 2020); and 4) Las Delicias volcanic series of northern Mexico, with zircon LA-ICPMS dates mostly clustered at 331 Ma and 270 Ma and a plutonic sample near Sierra El Granizo of 285 ± 3 Ma, whole rock ε_{Nd} values between +2.6 and +5.3, and T_{DM} model ages between 691 and 1502 Ma (Lopez, 1997). Early Permian volcaniclastic rocks in sedimentary successions deposited in forearc or intra-arc settings are well documented in several places in Mexico (e.g., Lopez, 1997; Mckee et al., 1988; Rosales-Lagarde et al., 2005). One of the examples is the lower Permian Tuzancoa Formation of east-central Mexico, which has a whole rock ε_{Nd} value of +4.4 and T_{DM} model age of 672 Ma and was suggested to be derived from a submarine continental arc (Rosales-Lagarde et al., 2005). Plutonic rocks in the Oaxaquia terrane were suggested to be continental arcs, caused by subduction of the Paleo-Pacific plate beneath western Pangea (e.g., Keppie et al., 2008; Nance et al., 2010; Kirsch et al., 2012) or Rheic plate beneath northern Gondwana (e.g., Elías-Herrera and Ortega-Gutiérrez, 2002; Vega-Granillo et al., 2007, 2009; Ortega-Obregón et al., 2014; Ortega-Gutiérrez et al., 2018; Coombs et al., 2020). The Las Delicias arc is also a continental arc formed by the subduction of the Laurentia plate beneath the Coahuila terrane (Lopez, 1997).

The ε_{Hf} signature supports that the Wolfcamp B tuffs ultimately sourced from the continental arc in the Peri-Gondwana realm. Zircons younger than 300 Ma in Wolfcamp B tuffs have an average ε_{Hf} value of +5.5 and T_{DM2} model ages between 675 and 1207 Ma, slightly different from those of the Mississippian tuffs with an average ε_{Hf} value of +2, and T_{DM2} between 682 and 1432 Ma. The isotopic signatures can be explained by mixing mantle-derived magmas and older continental crust (Arndt and Goldstein, 1987), similar to Mississippian tuffs that show the influence of Pan-African/Brasiliano and Grenville sources (Tian et al., 2022). The ε_{Hf} signature is also similar to the Cuanana pluton of the Acatlán metamorphic complex, which has a zircon ICP-MS date of 311 ± 2 Ma, ε_{Hf} values between +3 and +9, and T_{DM2} model ages between 795 and 948 Ma (Ortega-Obregón et al., 2014).

The interpretation that Wolfcamp B tuffs were ultimately sourced from a northern Gondwana arc is also supported because these tuffs contain 14% zircons between 500 and 850 Ma, which were ultimately sourced from Pan-African/Brasiliano basement, and 15% between 900 and 1300 Ma ultimately sourced from

Grenville basement (Fig. 6). The 500–850 Ma group has ε_{Hf} values ranging between −2.7 and +12.7, consistent with the signature of detrital Pan-African/Brasiliano zircons in Paleozoic sedimentary rocks on the Laurentian margin (e.g., Thomas et al., 2017; Waite et al., 2020). However, the two youngest zircons (525 ± 19 Ma and 553 ± 6 Ma) of this group could also be recycled from the Southern Oklahoma Aulacogen (SOA) related to the Iapetan rifting, because the ages and ε_{Hf} values are similar to those of SOA magmatic units (Thomas et al., 2016). Both the Oaxaquia and Coahuila terranes have Pan-African/Brasiliano and Grenville basement (Weber et al., 2010; Lopez et al., 2001). These *peri*-Gondwana terranes were close or attached to the southern Laurentia margin during the late Paleozoic because of Gondwana-Laurentia collision. Therefore, Wolfcamp B tuffs were most likely sourced from a continental arc on the Oaxaquia and Coahuila terranes.

The interpretation that Wolfcamp B tuffs were ultimately sourced from a northern Gondwana arc is further supported because the tuffs contain 50% zircons between 300 and 500 Ma with a peak at ~375 Ma (Fig. 10). The mode is not present in the detrital record of Laurentia before deposition of the Wolfcamp B unit (Fig. 11), and it is not reported in the Mississippian Stanley Group in the Ouachita Mountains (McGuire, 2017), Pennsylvanian sandstones in the Fort Worth Basin (Alsalem et al., 2018) and the Wolfcamp C unit in the Midland Basin (Liu and Stockli, 2020), suggesting that the zircon source of this age was not close to the Laurentia margin before Wolfcamp B deposition. Despite the fact that the Taconic, Acadian, and Alleghenian orogenesis in the Appalachians produced Paleozoic zircons, these only make a small portion in the lower Permian sedimentary rocks in the Appalachian foreland (e.g., Thomas et al., 2017), thus the Appalachians cannot be the ultimate source of Wolcamp B tuffs. However, Paleozoic zircons are common in the Mississippian Lower Santa Rosa Formation in southeastern Mexico (Weber et al., 2009). In addition to the Aserradero Rhyolite (348–340 Ma) near Ciudad Victoria, Mexico (Ramírez-Fernández et al., 2021), granitoids of 380–410 Ma and 371 ± 34 Ma were reported from the Acatlán Complex, southern Mexico (Yañez et al., 1991). Zircons of this age were also found in Pennsylvanian sedimentary rocks in the Arbuckle uplift in southern Oklahoma (Thomas et al., 2016) and the Marathon foreland in western Texas (Thomas et al., 2019); both were suggested to be derived from the Coahuila terrane (Fig. 1A). These ~375 Ma zircons have T_{DM2} model ages that mostly overlap with the Grenville Orogeny (900–1300 Ma), suggesting that the source was igneous material built on Grenville basement in the Peri-Gondwana realm. These zircons have an average εHf value of +2.8, similar to that of the Mississippian tuffs (Tian et al., 2022). Therefore, magmatism of ~375 Ma likely reflects early arc formation associated with subduction of the Rheic oceanic plate, and the dominance of 300–500 Ma zircons in Wolfcamp B tuffs suggests that these are most likely reworked tuffs and/or arc materials. If this interpretation is correct, the arrival of arc material by ~288 Ma, likely in the form of reworked tuffs delivered by rivers and deepwater gravity flows from northern Gondwana, may record the final stage of Gondwana-Laurentia collision and headwater erosion or catchment integration of northward-flowing rivers from highlands in northern Gondwana.

5.3.3. Wolfcamp A and Spraberry tuffs

Abundant unrounded zircons in the Wolfcamp A and Spraberry tuffs (Fig. 5) suggest that these tuffs have little detrital or inherited component. They also have similar ε_{Hf} signature (Fig. 10), suggesting that they may come from the same arc system. Magmatic units of similar age are also reported in the Oaxaquia terrane in southern Mexico. The best match for the Wolfcamp A tuff is the 287 ± 2 Ma Zanita Batholith, which has ε_{Hf} values between −4 and −1, and T_{DM2} ages between 1330 and 1550 Ma (Ortega-Obregón et al., 2014). Zúñiga et al. (2020) reported two groups of volcanic clasts in the Matzitzi Formation, southern Mexico. The intermediate group has zircon LA-ICPMS dates between 282 and 271 Ma, ε_{Hf} values between −8.1 and +0.2 and T_{DM2} ages between 1470 and

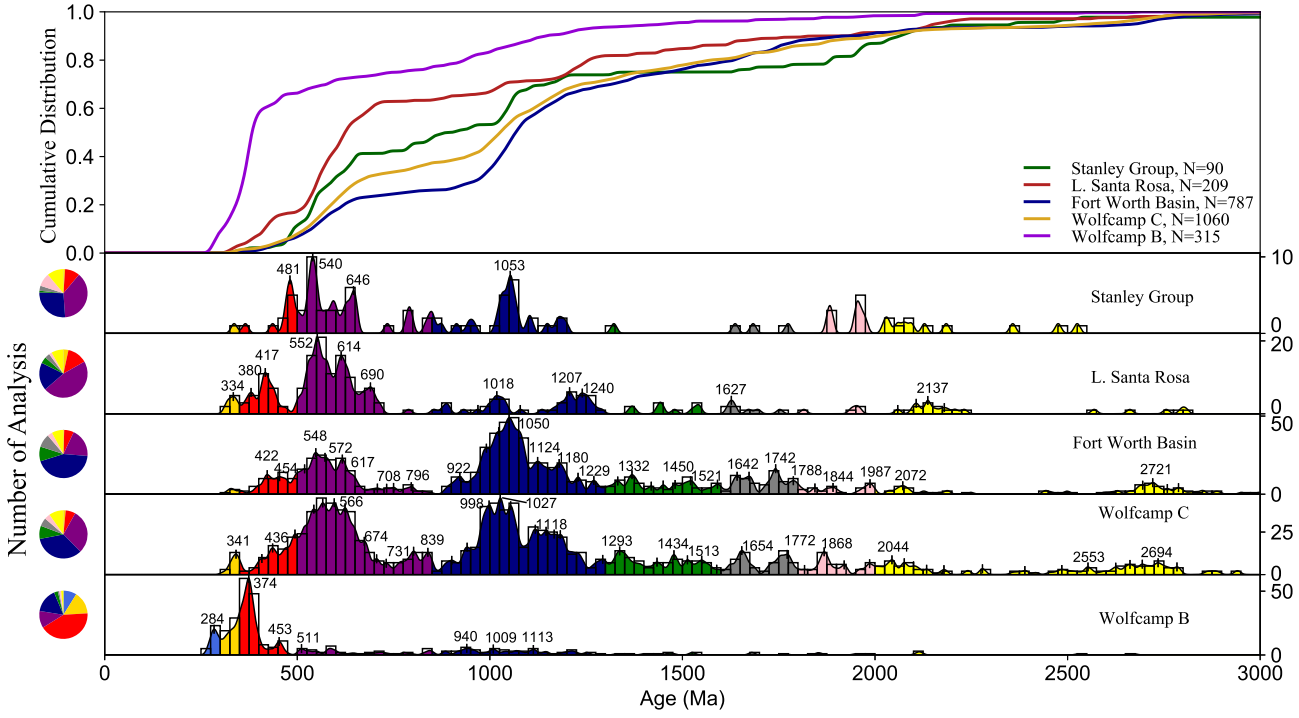

Fig. 11. LA-ICPMS U-Pb date distributions of detrital zircons near the study area. Data of the Late Mississippian Stanley Group are from McGuire (2017), the Late Mississippian Lower Santa Rosa Formation are from Weber et al. (2009), the Middle–Late Pennsylvanian strata in the Fort Worth Basin are from Alsalem et al. (2018), the Cisuralian Wolfcamp C unit are from Liu and Stockli (2020). The plot was shown as kernel density estimation. The numbers on the plot are peak modes. Data of the Lower Santa Rosa have 1σ uncertainty and all other data have 2σ uncertainty.

1520 Ma. This signature matches well with that of our Spraberry tuffs. The second group is ~281 Ma and has ε_{Hf} values between −3.6 and +8.4 (1 grain) and T_{DM2} ages between 1280 and 1320 Ma. The geochemical variability of these zircons suggests a heterogeneous parent melt caused by different mixtures of mantle-derived melts and Grenville basement. In southern Mexico, the Oaxaquia *peri*-Gondwana basement is 1200–1400 Ma, with ε_{Hf} values between +5 and +7 (Weber et al., 2010) (Fig. 10). Melting this basement decreases the ε_{Hf} values of parent magma. Therefore, Wolfcamp A and Spraberry tuffs were also most likely sourced from a continental arc on the Oaxaquia terrane.

5.3.4. Guadalupe Mountains tuffs

Magmatic units between 275 and 260 Ma are documented in southern Mexico (e.g., Ortega-Obregón et al., 2014), eastern Mexico (Coombs et al., 2020); northwestern Mexico (Riggs et al., 2016; Dobbs et al., 2021), and the Mojave Desert of California, USA (Cecil et al., 2019). These units may represent an ~N-S volcanic arc system formed by the eastward subduction of the Paleo-Pacific oceanic plate beneath the northwestern Gondwana (western Pangea arc) and southwestern Laurentia (Cordillera arc) (Fig. 1C). The arc system may have initiated at different times at different latitudes and the zircon ε_{Hf} signature of these arc magmas may have varied because different segments were built on crust of different ages and compositions. Zircon grains of 270–260 Ma on the Oaxaquia terrane in southern and eastern Mexico, including the Zaniza batholith and subsurface granitoids along the western Gulf of Mexico, have ε_{Hf} values between −16 and +0.2 (Ortega-Obregón et al., 2014; Coombs et al., 2020), more evolved than those from the Mojave Desert (ε_{Hf} values between −1.3 and +11.5) and our Guadalupian tuffs. Zircon grains of ~275 Ma in the Los Tanques pluton in Sonora, Mexico, also have more evolved ε_{Hf} signatures (average is −7.5) (Riggs et al., 2016) than our Guadalupian tuffs. Therefore, arc magmatism in southern and northwestern Mexico was not likely to be the source of the Guadalupian tuffs. Mojave Desert pluton zircons show a significant increase of ε_{Hf} values through time between 280 and 200 Ma, with the ε_{Hf} values of 280–260 Ma zircons between −5 and +10 (Cecil et al., 2019). The trend was suggested to reflect decreasing crustal contamination of mantle-derived melts through time because of extension and crustal thinning (Cecil et al., 2019). Therefore, it seems that the source of the Guadalupian tuffs is the Cordillera arc, most likely related to Mojave Desert plutons. Ash transport from volcano(es) about 1500 km to the west of the Texas may be facilitated by westerly winds at the low latitude of western equatorial Pangea (Tabor and Poulsen, 2008).

5.4. Implications for the late Paleozoic tectonics of southern Laurentia

It is debated whether late Cisuralian magmatisms discussed above reflect the final pulse of the northern Gondwana arc system formed by subduction of the Rheic oceanic plate (e.g., Elías-Herrera and Ortega-Gutiérrez, 2002; Vega-Granillo et al., 2007, 2009; Ortega-Gutiérrez et al., 2018) or the initiation of eastward subduction of the Paleo-Pacific oceanic plate beneath southwestern Pangea (e.g., Keppie et al., 2008; Nance et al., 2010). Our geochemical records show an abrupt change of mean zircon ε_{Hf} signature from +5.5 to −4.5 between Wolfcamp B and A tuffs that occurred near or within 1 Myr (between 288.2 and 287.2 Ma). A similar abrupt shift to evolved ε_{Hf} signature has been documented in Oaxaquia terrane magmatic rocks (Ortega-Obregón et al., 2014; Coombs et al., 2020). While Ortega-Obregón et al. (2014) attributed this to a change to more crustal contamination, Coombs et al. (2020) suggested that the juvenile signature was related to Rheic plate subduction that may have ended by ~286 Ma and the evolved signature (ε_{Hf} between −16 and −4), initiated by ~274 Ma, reflects late- or post-collisional magmatism influenced by Paleo-Pacific plate subduction. Furthermore, Zhao et al. (2020) suggested that magmatism in the Marathon segment ended by 270 Ma, as part of the late Paleozoic magmatism that ended diachronously from west to east along the Appalachian-Ouachita-Marathon belt, with the youngest magmatism was sourced from juvenile lower crust during post-orogenic slab break-off.

The geochemical similarity between magmatic zircons in the Wolfcamp B tuffs and the Mississippian Barnett tuff in the Midland Basin suggests that arc volcanism related to the subduction of the Rheic oceanic plate may have lasted until at least ~288 Ma (CA-ID-TIMS in this study) (Fig. 12). This is consistent with the inferred age of ~286 Ma (ICP-MS) from granitoid ε_{Hf} signatures in eastern Mexico (Coombs et al., 2020). This abrupt change of geochemical signature reflects a change of parent magma to a much more evolved composition that could have been caused by increased contribution from old continental crust, which can be achieved in four ways: 1) crustal thickening associated with subduction; 2) involvement of crust of different age and composition; 3) changing depth of magma evolution; and 4) formation of a new magmatic plumbing system for a new arc. While crustal thickening and underthrusting of lower crust into the melt source region are common in orogenic system, crustal assimilation is a gradual process and it takes at least 5 Myr to cause a major decrease in arc ε_{Hf} signature (e.g., DeCelles et al., 2009). Changing crustal composition of the northern Gondwana arc magmas also seems unlikely to be a cause of the abrupt isotope shift. Grains older than 500 Ma in the Wolfcamp A and B tuffs are mostly between 500–850 Ma and 900–1300 Ma, suggesting the sources of both tuffs have Pan-African/Brasiliano and Grenville basement. The sources should be *peri*-Gondwana terranes (i.e., Oaxaquia terrane) that have both Pan-African/Brasiliano and Grenville basement (Weber et al., 2010; Lopez et al., 2001). Zhao et al. (2020) suggested that magmatism in northern Gondwana may have lasted until ~270 Ma with the youngest magma derived from lower crust (Pan-African Orogeny materials) because of Rheic oceanic slab break-off. Changing from synorogenic to post-orogenic slab break-off magmatism cannot explain the observed abrupt isotopic shift because the ε_{Hf} signatures of Wolfcamp A-Spraberry zircons are more evolved than those of the ~326 Ma granitoids (+3.8 to +6.0) on the Maya *peri*-Gondwana terrane, which is suggested to reflect post-orogenic magmatism in the Ouachita segment (Zhao et al., 2020).

The abrupt isotopic change can be best explained by the termination of the northern Gondwana arc system and initiation of a new convergent margin along western Pangea associated with a new Paleo-Pacific plate subduction system (Fig. 12). The gradual increase of ε_{Hf} values from Wolfcamp A to Spraberry and Guadalupian tuffs (Fig. 10) is similar to the trend observed in the Mojave Desert pluton that was interpreted to be caused by diminishing sediment input as subduction of the Paleo-Pacific plate proceeded (Cecil et al., 2019). This similarity in ε_{Hf} trend, but difference in time between the magmatism in Mexico (~287 Ma) and Mojave Desert (~275 Ma) suggests that subduction of the Paleo-Pacific plate initiated at different times along the Laurentian margin. This age does not match well with the interpretation of Coombs et al. (2020), who suggested that the western Pangea arc, with negative ε_{Hf} values similar to those of our Wolfcamp A and Spraberry tuffs, initiated in Mexico by ~274 Ma. That study has a sampling gap for ~286–274 Ma, thus it could have missed the early initiation of the west Pangea arc.

Our results show that the late Cisuralian (~288 Ma) plate reorganization occurred very rapidly, near or less than 1 Myr. This reorganization was marked by the cessation of Laurentia-Gondwana collision that partly subducted the southern Laurentia margin beneath Gondwana, and the initiation of a new subduction zone along the southwestern Pangean margin. Our study thus confirms the inference that major plate reorganizations taking as little time

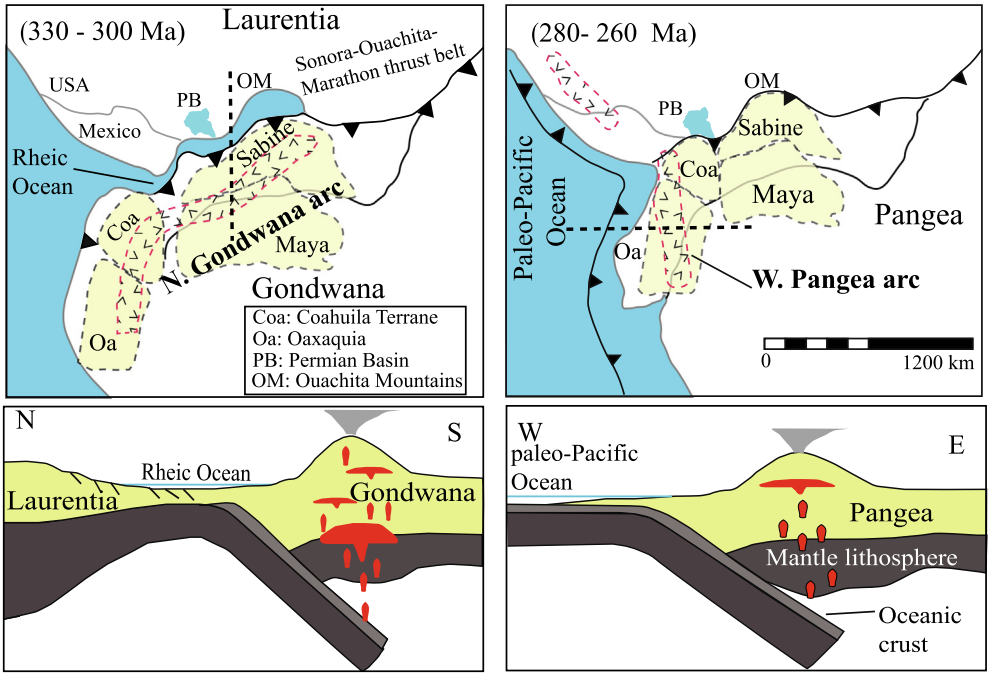

Fig. 12. Paleogeography reconstructions for two time periods after Ortega-Obregón et al. (2014) and Lawton et al. (2021). Thick black dash lines represent the locations of cross sections shown in the lower panel.

as less than a few million years are more likely caused by changes in plate motion due to plate margin creation or destruction (Richards and Lithgow-Bertelloni, 1996). Subduction of the Paleo-Pacific beneath western Gondwana may have caused the Permian-Triassic continental arc in eastern Mexico (e.g., Torres et al., 1999; Rosales-Lagarde et al., 2005; Coombs et al., 2020) and magmatic rocks of the Oaxacan and Acatlán metamorphic complexes in southwestern Mexico (Ortega-Obregón et al., 2014). The cessation of Pangea assembly changed the plate motion and promoted the northward propagation of the subduction system along western Pangea.

6. Conclusions

This study reports the first group of isotopic ages for early Permian tuffs in the Permian Basin and examines the geochemical and isotopic signatures of these tuffs and the Mississippian and Guadalupian tuffs in southern Laurentia to understand their magmatic affinities and tectonic significance. Our zircon CA-ID-TIMS dates show that the boundary between the Wolfcamp B and Wolfcamp A unit in the Midland Basin is ~287 Ma, which complements recent biostratigraphy results that correlate the Wolfcamp B unit to the late Sakmarian and early Artinskian stages, and the Wolfcamp A to the late Artinskian stage. Geochemical data of all these Mississippian-Permian tuffs and their zircons show continental arc signatures. Comparison of the geochemical data of these tuffs and magmatic units in Mexico and California further establishes the potential source of the tuffs on *peri*-Gondwana terranes in Mexico. The ε_{Hf} values abruptly change at ~287 Ma from higher, more juvenile signatures in the Mississippian and early Cisuralian Wolfcamp B tuffs to consistently negative ε_{Hf} values in the Cisuralian Wolfcamp A and Spraberry tuffs. At the same time, a higher proportion of more angular zircons appear in the tuffs and the proportion of detrital zircons decreases. The ~288 Ma zircon signature shift between 288.2 and 287.2 Ma is best explained by the termination of the northern Gondwana arc system related to subduction of the Rheic oceanic plate and initiation of a western Pangea arc system related to subduction of the Paleo-Pacific oceanic plate.

In addition to the chronostratigraphy and tectonic significance, the comparison of LA-ICPMS dates derived from different statistical approaches and the true depositional ages of the tuffs determined by CA-ID-TIMS zircon dating offers important new insights to better understand the limitation of LA-ICPMS zircon ages. Several commonly used statistical approachs, including the weighted mean date of the youngest cluster of three or more grains overlapping at 2σ error (YSP), weighted mean date of the youngest mode from KDE (WMKDE), and TuffZirc date all are too young, but within 96% of the true depositional ages, thus can be used to approximate true depositional age if CA-ID-TIMS ages are not available. The newly defined, weighted mean date of the youngest dominant KDE mode (WMYDM) is closest to the true depositional age, and the small difference between this date and true depositional age may reflect the skewness of the LA-ICPMS zircon age distribution. Chemical abrasion pre-treatment or simply annealing zircons prior to LA-ICPMS analysis may greatly improve the accuracy of the LA-ICPMS method in assessing true depositional ages from tuffs.

CRediT authorship contribution statement

Hepeng Tian: Writing – original draft, Investigation, Visualization. **Majie Fan:** Writing – review & editing, Conceptualization, Supervision. **Valencia Victor:** Data curation, Writing – review & editing. **Kevin Chamberlain:** Data curation, Writing – review & editing. **Lowell Waite:** Resources, Writing – review & editing. **Robert J. Stern:** Writing – review & editing. **Matthew Loocke:** Data curation, Writing – review & editing.

Declaration of Competing Interest

The authors declare that they have no known competing financial interests or personal relationships that could have appeared to influence the work reported in this paper.

Acknowledgements

We thank Pioneer Natural Resources for providing us tuff samples and initial funding, and the Gulf Coast Association of Geological Societies for additional financial support. We also thank Dr. Jonena Hearst from Guadalupe Mountains National Park for helping with sampling and Dr. Xiangyang Xie from Texas Christian University for letting us use his mineral separation facility. Comments from two anonymous reviewers and Dr. Timothy Lawton greatly improved the work. This is UTD Geoscience Dept. contribution # 1684 and Permian Basin Research Lab contribution #4.

Appendix A. Supplementary material

Supplementary data to this article can be found online at https://doi.org/10.1016/j.gr.2022.07.003.

References

Adams, J.E., 1965. Stratigraphic-tectonic development of Delaware Basin, West Texas and southeastern New Mexico. AAPG Bull. 49, 2140–2148.

Adams, J.E., Cheney, M.G., Deford, R.K., Dickey, R.I., Dunbar, C.O., Hills, J.M., King, R. E., Lloyd, E.R., Miller, A.K., Needham, C.E., 1939. Standard Permian Section of North America. AAPG Bull. 23, 1673–1678. https://doi.org/10.1306/3D933136-16B1-11D7-8645000102C1865D.

Allen, C.M., Campbell, I.H., 2012. Identification and elimination of a matrix-induced systematic error in LA-ICP-MS $^{206}P/^{238}U$ dating of zircon. Chem. Geol. 333, 157–165.

Alsalem, O.B., Fan, M., Zamora, J., Xie, X., Griffin, W.R., 2018. Paleozoic sediment dispersal before and during the collision between Laurentia and Gondwana in the Fort Worth Basin, USA. Geosphere 14 (1), 325–342.

Anderson, D.L., 2001. Top-Down Tectonics? Science 293 (5537), 2016–2018.

Arndt, N.T., Goldstein, S.L., 1987. Use and abuse of crust-formation ages. Geology 15, 893–895. https://doi.org/10.1130/0091-7613(1987)15<893:UAAOCA>2.0.CO;2.

Baumgardner, R.W., Hamlin, H.S., Rowe, H., 2016. Lithofacies of the Wolfcamp and lower Leonard intervals, southern Midland Basin, Texas. The University of Texas at Austin, Bureau of Economic Geology, Report of Investigations 281, 67.

Behnken, F.H., 1984. Conodont biostratigraphy of the Wolfcampian Series Standard Section (Lower Permian, Sakmarian) Wolfcamp Hills, west Texas. Geol. Soc. America - Abstracts Programs 16, 124.

Belousova, E., Griffin, W., O'Reilly, S.Y., Fisher, N., 2002. Igneous zircon: trace element composition as an indicator of source rock type. Contrib. Mineral. Petrol. 143 (5), 602–622.

Cawood, P.A., Hawkesworth, C.J., Dhuime, B., 2012. Detrital zircon record and tectonic setting. Geology 40, 875–878. https://doi.org/10.1130/G32945.1.

Cecil, M.R., Ferrer, M.A., Riggs, N.R., Marsaglia, K.M., Kyland-er-Clark, A., Ducea, M. N., Stone, P., 2019. Early arc development recorded in Permian-Triassic plutons of the northern Mojave Desert region, California, USA. Geol. Soc. Am. Bull. 131, 749–765. https://doi.org/10.1130/B31963.1.

Chernykh, V.V., Ritter, S.M., 1997. Streptognathodus (Conodonta) Succession at the Proposed Carboniferous-Permian Boundary Stratotype Section, Aidaralash Creek, Northern Kazakhstan. J. Paleontol. 71 (3), 459–474.

Chernykh, V.V., Chuvashov, B.I., Davydov, V.I., Schmitz, M., Snyder, W.S., 2006. Usolka section (southern Urals, Russia): A potential candidate for GSSP to define the base of the Gzhelian Stage in the global chronostratigraphic scale. Geologija 49 (2), 205–217.

Chuvashov, B.I., Chernykh, V.V., Shen, S., Henderson, C.M., 2013. Proposal for the Global Stratotype Section and Point (GSSP) for the base-Artinskian Stage (Lower Permian). Permophiles 58, 26–34.

Chuvashov, B.I., Chernykh, V.V., Leven, E.Y., Davydov, V.I., Bowring, S., Ramezani, J., Glenister, B.F., Henderson, C., Schiappa, T.A., Northrup, C.J., Snyder, W.S., Spinosa, C., Wardlaw, B.R., 2002. Progress report on the base of the Artinskian and base of the Kungurian by the Cisuralian Working Group. Permophiles 41, 13–16.

Coombs, H.E., Kerr, A.C., Pindell, J., Buchs, D., Weber, B., Solari, L., 2020. Petrogenesis of the crystalline basement along the western Gulf of Mexico: Post-collisional magmatism during the formation of Pangea. In: Martens, U., Molina Garza, R.S. (Eds.), Southern and Central Mexico: Basement Framework, Tectonic Evolution, and Provenance of Mesozoic–Cenozoic Basins: Geological Society of America Special Paper 546, pp. 29–52.

Coutts, D.S., Matthews, W.A., Hubbard, S.M., 2019. Assessment of widely used methods to derive depositional ages from detrital zircon populations. Geosci. Front. 10 (4), 1421–1435. https://doi.org/10.1016/j.gsf.2018.11.002.

Crowell, J.C., 1978. Gondwanan glaciation, cyclothems, continental positioning and climate change. Am. J. Sci. 278 (10), 1345–1372.

Davies, T.A., Hay, W.W., Southam, J.R., Worsley, T.R., 1977. Estimates of Cenozoic Oceanic Sedimentation Rates. Science 197 (4298), 53–55.

Davydov, V.I., Glenister, B.F., Spinosa, C., Ritter, S.M., Chernykh, V.V., Wardlaw, B.R., Snyder, W.S., 1998. Proposal of Aidaralash as Global Stratotype Section and Point (GSSP) for base of the Permian System. Episodes 21 (1), 11–18.

DeCelles, P.G., Ducea, M.N., Kapp, P., Zandt, G., 2009. Cyclicity in Cordilleran orogenic systems. Nat. Geosci. 2 (4), 251–257.

Dhuime, B., Hawkesworth, C., Cawood, P., 2011. When Continents Formed. Science 331 (6014), 154–155.

Dickinson, W.R., Gehrels, G.E., 2009. Use of U – Pb ages of detrital zircons to infer maximum depositional ages of strata: A test against a Colorado Plateau Mesozoic database. Earth Planet. Sci. Lett. 288, 115–125. https://doi.org/10.1016/j.epsl.2009.09.013.

Dobbs, S.C., Riggs, N.R., Marsaglia, K.M., González-León, G.M., Cecil, M.R., Smith, M. E., 2021. The Permian Monos Formation: Stratigraphic and detrital zircon evidence for Permian Cordilleran arc development along the southwestern margin of Laurentia (northwestern Sonora, Mexico). Geosphere 17, 520–537.

Domeier, M., Torsvik, T.H., 2014. Plate tectonics in the late Paleozoic. Geosci. Front. 5 (3), 303–350.

Dutton, S.P., Kim, E.M., Broadhead, R.F., Raatz, W.D., Breton, C.L., Ruppel, S.C., Kerans, C., 2005. Play analysis and leading-edge oil-reservoir development methods in the Permian Basin: Increased recovery through advanced technologies. AAPG Bull. 89 (5), 553–576.

Elías-Herrera, M., Ortega-Gutiérrez, F., 2002. Caltepec fault zone: an early Permian dextral transpressional boundary between the Proterozoic Oaxacan and Paleozoic Acatlán complexes, southern Mexico, and regional tectonic implications. Tectonics 21 (3), 4-1–4-18.

Estrada-Carmona, J., Weber, B., Scherer, E.E., Martens, U., Elías-Herrera, M., 2016. Lu-Hf geochronology of Mississippian high-pressure metamorphism in the Acatlán Complex, southern México. Gondwana Res. 34, 174–186.

Gärtner, A., Linnemann, U., Sagawe, A., Hofmann, M., Ullrich, B., Kleber, A., 2013. Morphology of zircon crystal grains in sediments – characteristics, classifications, definitions. Cent. Eur. Geol. 59, 65–73.

Gehrels, G., 2014. Detrital Zircon U-Pb Geochronology Applied to Tectonics. Annu. Rev. Earth Planet. Sci. 42 (1), 127–149. https://doi.org/10.1146/annurev-earth-050212-124012.

Glenister, B.F., Boyd, D.W., Furnish, W.M., Grant, R.E., Harris, M.T., Kozur, H., Lambert, L.L., Nassichuk, W.W., Newell, N.D., Pray, L.C., Spinosa, C., Wardlaw, B. R., Wilde, G.L., Yancey, T.E., 1992. The Guadalupian: proposed international standard for a middle Permian series. Int. Geol. Rev. 34 (9), 857–888.

Glenister, B.F., Wardlaw, B.R., Lambert, L.L., Spinosa, C., Bowring, S.A., Erwin, D.H., Menning, M., Wilde, G.L., 1999. Proposal of Guadalupian and component Roadian, Wordian, and Capitanian Stages as international standards for the middle Permian Series. Permophiles 34, 3–11.

Griffin, W.L., Wang, X., Jackson, S.E., Pearson, N.J., O'Reilly, S.Y., Xu, X., Zhou, X., 2002. Zircon chemistry and magma mixing, SE China: in-situ analysis of Hf isotopes, Pingtan and Tonglu igneous complexes. Lithos 61, 237–269.

Grimes, C.B., Wooden, J.L., Cheadle, M.J., John, B., 2015. "Fingerprinting" tectono-magmatic provenance using trace elements in igneous zircon. Contrib. Mineral. Petrol. 170, 1–26.

Hamlin, H.S., Baumgardner, R.W., 2012. Wolfberry (Wolfcampian-Leonardian) Deep-water Depositional Systems in the Midland Basin: Stratigraphy, Lithofacies, Reservoirs, and Source Rocks. The University of Texas at Austin, Bureau of Economic Geology, Report of Investigations 277, 1-61.

Handford, C., 1981. Sedimentology and Genetic Stratigraphy of Dean and Spraberry Formations (Permian), Midland Basin, Texas. AAPG Bull. 65, 1602–1616. https://doi.org/10.1306/03B5962A-16D1-11D7-8645000102C1865D.

Heckel, P.H., Clayton, G., 2006. The Carboniferous System. Use of the new official names for the subsystems, series, and stages. Geol. Acta 4, 403–407. https://doi.org/10.1016/S0016-7878(06)80045-3.

Henderson, C.M., Wardlaw, B.R., Davydov, V.I., Schmitz, M.D., Schiappa, T.A., Tierney, K.E., Shen, S., 2012. Proposal for base-Kungurian GSSP. Permophiles 56, 8–21.

Herriott, T.M., Crowley, J.L., Schmitz, M.D., Wartes, M.A., Gillis, R.J., 2019. Exploring the law of detrital zircon: LA-ICP-MS and CA-TIMS geochronology of Jurassic forearc strata. Geology 47, 1044–1048.

Hill, C.A., 1996. Geology of the Delaware Basin, Guadalupe, Apache and Glass Mountains, New Mexico and West Texas. Society of Economic Mineralogists and Paleontologists, Permian Basin Section 96-39, 1-480.

Jones, R.E., Kirstein, L.A., Kasemann, S.A., Dhuime, B., Elliott, T., Litvak, V.D., Alonso, R., Hinton, R., 2015. Geodynamic controls on the contamination of Cenozoic arc magmas in the southern Central Andes: Insights from the O and Hf isotopic composition of zircon. Geochim. Cosmochim. Acta 164, 386–402.

Keppie, J., Dostal, J., Murphy, J., Nance, R., 2008. Synthesis and tectonic interpretation of the westernmost Paleozoic Variscan orogen in southern Mexico: from rifted Rheic margin to active Pacific margin. Tectonophysics 461, 277–290. https://doi.org/10.1016/j. tecto.2008.01.012.

King, S.D., Lowman, J.P., Gable, C.W., 2002. Episodic tectonic plate reorganizations driven by mantle convection. Earth Planet. Sci. Lett. 203 (1), 83–91.

Kirsch, M., Keppie, J.D., Murphy, J.B., Solari, L.A., 2012. Permian-Carboniferous arc magmatism and basin evolution along the western margin of Pangea: geochemical and geochronological evidence from the eastern Acatlán Complex, southern Mexico. Geol. Soc. Am. Bull. 124, 1607–1628. https://doi.org/10.1130/B30649.1.

Kohn, J., Barrick, J.E., Wahlman, G.P., Baumgardner, R., 2019. Late Pennsylvanian (Virgilian) to early Permian (Leonardian) conodont biostratigraphy of the "Wolfcamp Shale," northern Midland Basin, Texas. In: Denne, R.A., Kahn, A. (Eds.), Geologic Problem Solving with Microfossils IV. SEPM Special Publication, pp. 245–261. https://doi.org/10.2110/sepmsp.111.11.

Lawton, T.F., Blakey, R.C., Stockli, D.F., Liu, L., 2021. Late Paleozoic (Late Mississippian-middle Permian) sediment provenance and dispersal in western

equatorial Pangea. Palaeogeogr. Palaeoclimatol. Palaeoecol. 572, 1–35. https://doi.org/10.1016/j.palaeo.2021.110386.
Leary, R.J., Umhoefer, P., Smith, M.E., Riggs, N., 2017. A three-sided orogen: A new tectonic model for Ancestral Rocky Mountain uplift and basin development. Geology 45, 735–738. https://doi.org/10.1130/G39041.1.
Liu, L., Stockli, D.F., 2020. U-Pb ages of detrital zircons in lower Permian sandstone and siltstone of the Permian basin, west Texas, USA: Evidence of dominant Gondwanan and peri-Gondwanand sediment input to Laurentia. Geol. Soc. Am. Bull. 132, 245–262. https://doi.org/10.1130/B35119.1.
Lopez, R., 1997. The pre-Jurassic geotectonic evolution of the Coahuila terrane, northwestern Mexico: Grenville basement, a late Paleozoic arc: Triassic plutonism, and the events south of the Ouachita suture. Ph.D. thesis. University of California.
Lopez, R., Cameron, K.L., Jones, N.W., 2001. Evidence for Paleoproterozoic, Grenvillian, and Pan-African age Gondwanan crust beneath northeastern Mexico. Precambrian Res. 107 (3-4), 195–214.
Lucas, S.G., Shen, S.-Z., 2018. The Permian timescale: an introduction. Geol. Soc. Lond. Spec. Publ. 450 (1), 1–19.
Ludwig, K.R., 2008. User's Manual for Isoplot 3.70. Berkeley Geochronology Center Special Publication, 76.
Ludwig, K.R., Mundil, R., 2002. Extracting reliable U-Pb ages and errors from complex populations of zircons from Phanerozoic tuffs. Geochim. Cosmochim. Acta 66 (15A), 463.
Mallard, C., Coltice, N., Seton, M., Müller, R.D., Tackley, P.J., 2016. Subduction controls the distribution and fragmentation of Earth's tectonic plates. Nature 535 (7610), 140–143.
Marantos, I., Markopoulos, T.h., Christidis, G.E., Perdikatsis, V., 2008. Geochemical characteristics of the alteration of volcanic and volcaniclastic rocks in the Feres Basin, Thrace, NE Greece. Clay miner. 43 (4), 575–595.
Matthews, K.J., Seton, M., Müller, R.D., 2012. A global-scale plate reorganization event at 105–100 Ma. Earth Planet. Sci. Lett. 355-356, 283–298.
Mattinson, J.M., 2005. Zircon U-Pb chemical abrasion ("CA-TIMS") method: Combined annealing and multi-step partial dissolution analysis for improved precision and accuracy of zircon ages. Chem. Geol. 220 (1-2), 47–66.
Mazzullo, S.J., 1982. Stratigraphy and Depositional Mosaics of Lower Clear Fork and Wichita Groups (Permian), Northern Midland Basin, Texas. AAPG Bull. 66, 210–227.
Mazzullo, S.J., Reid, A.M., Mazzullo, L.J., 1987. Basinal Lower Permian Facies, Permian Basin: Part I - Stratigraphy of the Wolfcampian-Leonardian Boundary. W. Tex. Geol. Soc. Bull. 26, 5–9.
Mazzullo, S.J., Reid, A.M., 1989. Lower Permian Platform And Basin Depositional Systems, Northern Midland Basin, Texas. In: Crevello, P.D., Wilson, J.L., Sarg, J.F., Read, J.F. (Eds.), Controls on Carbonate Platforms and Basin Development. SEPM Society for Sedimentary Geology, pp. 305–320. https://doi.org/10.2110/pec.89.44.0305.
McGuire, P.R., 2017. U-Pb detrital zircon signature of the Ouachita orogenic belt. M. S. thesis. Texas Christian University.
Mckee, J.W., Jones, N.W., Anderson, T.H., 1988. La Delicias basin: a record of late Paleozoic arc volcanism in northeastern Mexico. Geology 16, 37–40. https://doi.org/10.1130/0091-7613(1988)016,0037:LDBARO.2.3.CO;2.
Montgomery, S.L., 1996. Permian "Wolfcamp" Limestone Reservoirs: Powell Ranch Field, Eastern Midland Basin. AAPG Bull. 80, 1349–1365. https://doi.org/10.1306/64ED9A38-1724-11D7-8645000102C1865D.
Morra, G., Seton, M., Quevedo, L., Müller, R.D., 2013. Organization of the tectonic plates in the last 200 Myr. Earth Planet. Sci. Lett. 373, 93–101.
Murakami, H., Ishihara, S., 2008. REE Mineralization of Weathered Crust and Clay Sediment on Granitic Rocks in the Sanyo Belt, SW Japan and the Southern Jiangxi Province, China. Resour. Geol. 58 (4), 373–401.
Nance, R.D., Linnemann, U., 2008. The Rheic Ocean: Origin, Evolution, and Significance. GSA Today 18, 4–12.
Nance, R.D., Gutiérrez-Alonso, G., Keppie, J.D., Linnemann, U., Murphy, J.B., Quesada, C., Strachan, R.A., Woodcock, N.H., 2010. Evolution of the Rheic Ocean. Gondwana Res. 17 (2-3), 194–222. https://doi.org/10.1016/j.gr.2009.08.001.
Nicklen, B., Gorden, J., Lance, L., Warren, H., 2015. Tephrochronology of the Manzanita Limestone in the Middle Permian (Guadalupian) Type Area, West Texas and southeastern New Mexico, USA. Stratigraphy 12, 123–147.
McDonough, W.F., Sun, S.S., 1995. The composition of the Earth. Chemical Geology 120, 223–253.
Ortega-Gutiérrez, F., Elías-Herrera, M., Morán-Zenteno, D.J., Solari, L., Weber, B., Luna-González, L., 2018. The pre-Mesozoic metamorphic basement of Mexico, 1.5 billion years of crustal evolution. Earth Sci. Rev. 183, 2–37. https://doi.org/10.1016/j.earscirev.2018.03.006.
Ortega-Obregón, C., Solari, L., Gómez-Tuena, A., Elías-Herrera, M., Ortega-Gutiérrez, F., Macías-Romo, C., 2014. Permian-Carboniferous arc magmatism in southern Mexico: U-Pb dating, trace element and Hf isotopic evidence on zircons of earliest subduction beneath the western margin of Gondwana. Int. J. Earth Sci. 103 (5), 1287–1300.
Pearce, J.A., Harris, N.B.W., Tindle, A.G., 1984. Trace Element Discrimination Diagrams for the Tectonic Interpretation of Granitic Rocks. J. Petrol. 25 (4), 956–983.
Peccerillo, A., Taylor, S.R., 1976. Geochemistry of Eocene calc-alkaline volcanic rocks from the Kastamonu area, Northern Turkey. Contrib. Mineral. Petrol. 58 (1), 63–81.
Poole, F.G., Perry William, J.J., Madrid, R.J., Amaya-Martínez, R., 2005. Tectonic synthesis of the Ouachita-Marathon-Sonora orogenic margin of southern Laurentia. In: Anderson, T.H., Nourse, J.A., McKee, J.W., Steiner, M.B. (Eds.), Stratigraphic and structural implications for timing of deformational events and plate-tectonic model. Geol. Soc. Am. Spec. Pap. 393, 543–596. doi: 10.1130/0-8137-2393-0.543.
Ramezani, J., Bowring, S.A., 2018. Advances in numerical calibration of the Permian timescale based on radioisotopic geochronology. In: Lucas, S.G., Shen, S. (Eds.), The Permian Times. Geol. Soc. Lond. Spec. Publ. 450, 51–60. doi: 10.1144/SP450.17.
Ramírez-Fernández, J.A., Alemán-Gallardo, E.A., Cruz-Castillo, D., Velasco-Tapia, F., Jenchen, U., Becchio, R., De León-Barragán, L., Casas-Peña, J.M., 2021. Early Mississippian precollisional, peri-Gondwanan volcanic arc in NE-Mexico: Aserradero Rhyolite from Ciudad Victoria, Tamaulipas. Int. J. Earth Sci. 110 (7), 2435–2463.
Richards, M.A., Lithgow-Bertelloni, C., 1996. Plate motion changes, the Hawaiian-Emperor bend, and the apparent success and failure of geodynamic models. Earth Planet. Sci. Lett. 137 (1-4), 19–27.
Riggs, N.R., Barth, A.P., Walker, J.D., Lindner, P., Gonzalez- Leon, C., Cecil, M.R., Marsaglia, K.M., 2016. Implications of Permian magmatism in south-west Laurentia for tectonic reconstructions. Geol. Soc. America Abstracts Programs 48 (7). https://doi.org/10.1130/abs/2016AM-279985.
Rosales-Lagarde, L., Centeno-García, E., Dostal, J., Sour-Tovar, F., Ochoa-Camarillo, H., Quiroz-Barroso, S., 2005. The Tuzancoa Formation: evidence of an Early Permian submarine continental arc in east-central Mexico. Int. Geol. Rev. 47 (9), 901–919.
Ross, C.A., 1986. Paleozoic evolution of southern margin of Permian Basin. Geol. Soc. Am. Bull. 97, 536–554. https://doi.org/10.1130/0016-7606(1986)97<536.
Ross, C.A., Ross, J.R.P., 2003. Fusulinid sequence evolution and sequence extinction in Wolfcampian and Leonardian Series (Lower Permian), Glass Mountains, West Texas. Riv. Ital. Paleontol. Stratigr. 109, 281–306.
Ross, C.A., Ross, J.R.P., 2009. Paleontology, a tool to resolve late Paleozoic structural and depositional histories. SEPM Special Publication 93, 93–110.
Rudnick, R.L., Gao, S., 2003. Composition of the continental crust. In: Rudnick, R.L. (Ed.), Treatise on Geochemistry, Volume 4: The Crust. Elsevier, Oxford, UK, pp. 1–64. https://doi.org/10.1016/B0-08-043751-6/03016-4.
Schaltegger, U., Schmitt, A.K., Horstwood, M.S.A., 2015. U-Th-Pb zircon geochronology by ID-TIMS, SIMS, and laser ablation ICP-MS: recipes, interpretations, and opportunities. Chem. Geol. 402, 89–110. https://doi.org/10.1016/j.chemgeo.2015.02.028.
Schmid, R., 1981. Descriptive nomenclature and classification of pyroclastic deposits and fragments: Recommendations of the IUGS Subcommission on the Systematics of Igneous Rocks. Geology 9 (1), 41. https://doi.org/10.1130/0091-7613(1981)9<41:DNACOP>2.0.CO;2.
Schoene, B., 2014. U-Th–Pb Geochronology. In: Rudnick, R.L. (Ed.), Treatise on Geochemistry (second edition), Volume 4: The Crust. Elsevier, Oxford, UK, pp. 341–378. https://doi.org/10.1016/B978-0-08-095975-7.00310-7.
Silver, B.A., Todd, R.G., 1969. Permian Cyclic Strata, Northern Midland and Delaware Basins, West Texas and Southeastern New Mexico. AAPG Bull. 53, 2223–2251. https://doi.org/10.1306/5d25c94d-16c1-11d7-8645000102c1865d.
Spencer, C.J., Kirkland, C.L., Taylor, R.J.M., 2016. Strategies towards statistically robust interpretations of in situ U e Pb zircon geochronology. Geosci. Front. 7, 581–589. https://doi.org/10.1016/j.gsf.2015.11.006.
Susn, W., McDonough, W.F., 1989. Chemical and isotopic systematics of oceanic basalts: Implications for mantle composition and processes. Geol. Soc. Lond. Spec. Publ. 42 (1), 313–345. https://doi.org/10.1144/GSL.SP.1989.042.01.19.
Tabor, N.J., Poulsen, C.J., 2008. Palaeoclimate across the Late Pennsylvanian-Early Permian tropical palaeolatitudes: A review of climate indicators, their distribution, and relation to palaeophysiographic climate factors. Palaeogeogr. Palaeoclimatol. Palaeoecol. 268 (3-4), 293–310.
Thomas, W.A., Gehrels, G.E., Lawton, T.F., Satterfield, J.I., Romero, M.C., Sundell, K.E., 2019. Detrital zircons and sediment dispersal from the Coahuila terrane of northern Mexico into the Marathon foreland of the southern Mid-continent. Geosphere 15, 1102–1127. https://doi.org/10.1130/GES02033.1.
Thomas, W.A., Gehrels, G.E., Romero, M.C., 2016. Detrital zircons from crystalline rocks along the Southern Oklahoma fault system, Wichita and Arbuckle Mountains, USA. Geosphere 12 (4), 1224–1234.
Thomas, W.A., Gehrels, G.E., Greb, S.F., Nadon, G.C., Satkoski, A.M., Romero, M.C., 2017. Detrital zircons and sediment dispersal in the Appalachian foreland. Geosphere 13, 2206–2230. https://doi.org/10.1130/GES01525.1.
Tian, H., Fan, M., Valencia, V., Chamberlain, K., Waite, L., Stern, R.J., 2022. Mississippian Laurentian tuffs came from a northern Gondwana arc. Geology. https://doi.org/10.1130/G49502.1.
Torres, R., Ruiz, J., Patchett, P.J., and Grajales-Nishimura, J.M., 1999. Permo-Triassic continental arc in eastern Mexico; tectonic implications for reconstructions of southern North America. In: Bartolini, C., Wilson, J.L., Lawton, T.F. (Eds.), Mesozoic Sedimentary and Tectonic History of North-Central Mexico. Geol. Soc. Am. Spec. Pap. 340, 191–196.
Vega-Granillo, R., Talavera-Mendoza, O., Meza-Figueroa, D., Ruiz, J., Gehrels, G.E., López-Martínez, M., de La Cruz-Vargas, J.C., 2007. Pressure–temperature–time evolution of Paleozoic high-pressure rocks of the Acatlán Complex (southern Mexico): implications for the evolution of the Iapetus and Rheic Oceans. Geol. Soc. Am. Bull. 119, 1249–1264. https://doi.org/10.1130/B226031.1.
Vega-Granillo, R., Calmus, T., Meza-Figueroa, D., Ruiz, J., Talavera-Mendoza, O., López-Martínez, M., 2009. Structural and tectonic evolution of the Acatlán Complex, southern Mexico: its role in the collisional history of Laurentia and Gondwana. Tectonics 28, TC4008. https://doi.org/10.1029/2007TC002159.
Vermeesch, P., 2012. On the visualisation of detrital age distributions. Chem. Geol. 312, 190–194. https://doi.org/10.1016/j.chemgeo.2012.04.021.

Wahlman, G.P., 2013. Pennsylvanian to Lower Permian (Desmoinesian – Wolfcampian) fusulinid biostratigraphy of Midcontinent North America. Stratigraphy 10, 73–104.

Wahlman, G.P., Barrick, J., Baumgardner, W., 2016. Fusulinid and conodont biostratigraphy of the "Wolfcamp Shale" in the Midland Basin, West Texas: a progress report. West Texas Geological Society 2016 Fall Symposium, WTGS Special Publication 16-32.

Waite, L., Fan, M., Collins, D., Gehrels, G., Stern, R.J., 2020. Detrital zircon provenance evidence for an early Permian longitudi-nal river flowing into the Midland Basin of west Texas. Int. Geol. Rev. 62, 1–21. https://doi.org/10.1080/00206814.2020.1756930.

Wardlaw, B.R., Davydov, V.I., 2000. Preliminary Placement of the International Lower Permian working Standard to the Glass Mountains, Texas. Permophiles 36, 11–14.

Wardlaw, B.R., Nestell, M.K., 2014. The first appearance of Streptognathodus isolatus in the Permian of Texas. Permophiles 59, 17–19.

Weber, B., Valencia, V.A., Schaaf, P., Ortega-Gutiérrez, F., 2009. Detrital zircon ages from the Lower Santa Rosa Formation, Chiapas: Implications on regional Paleozoic stratigraphy. Revista Mexicana de Ciencias Geológicas 26, 260–276.

Weber, B., Scherer, E.E., Schulze, C., Valencia, V.A., Montecinos, P., Mezger, K., Ruiz, J., 2010. U-Pb and Lu–Hf isotope systematics of lower crust from central–southern Mexico–geodynamic significance of Oaxaquia in a Rodinia realm. Precambrian Res. 182 (1-2), 149–162.

Wilde, G.L., 1975. Fusulinid-defined Permian stages. Permian Exploration Boundaries and Stratigraphy. West Texas Geological Society and Permian Basin Section, Publication, 65–75.

Wilde, G.L., 1990. Practical fusulinid zonation: the species concept; with Permian Basin emphasis. W. Tex. Geol. Soc. Bull. 44, 5–34.

Winchester, J.A., Floyd, P.A., 1977. Geochemical discrimination of different magma series and their differentiation products using immobile elements. Chem. Geol. 20, 325–343. https://doi.org/10.1016/0009-2541(77)90057-2.

Workman, R.K., Hart, S.R., 2005. Major and trace element composition of the depleted MORB mantle (DMM). Earth Planet. Sci. Lett. 231 (1-2), 53–72.

Wu, Q., Ramezani, J., Zhang, H., Yuan, D.-X., Erwin, D.H., Henderson, C.M., Lambert, L. L., Zhang, Y.-C., Shen, S.-Z., 2020. High-precision U-Pb zircon age constraints on the Guadalupian in West Texas, USA. Palaeogeogr. Palaeoclimatol. Palaeoecol. 548, 109668. https://doi.org/10.1016/j.palaeo.2020.109668.

Yañez, P., Patchett, P.J., Ortega-Gutiérrez, F., Gehrels, G.E., 1991. Isotopic studies of the Acatlán Complex, southern Mexico: Implications for Paleozoic North American tectonics. Geol. Soc. Am. Bull. 103, 817–828. https://doi.org/10.1130/0016-7606 (1991)103<0817:ISOTAC>2.3.CO;2.

Yang, K.M., Dorobek, S., 1995. The Permian Basin of West Texas and New Mexico: Flexural Modeling and Evidence for Lithospheric Heterogeneity across the Marathon Foreland. In: Dorobek, S.L., Ross, G.M. (Eds.), Stratigraphic Evolution of Foreland Basins. doi: 10.2110/pec.95.52.0037.

Zhao, J., Xiao, L., Gulick, S.P.S., Morgan, J.V., Kring, D., Fucugauchi, J.U., Schmieder, M., de Graaf, S.J., Wittmann, A., Ross, C.H., Claeys, P., Pickersgill, A., Kaskes, P., Goderis, S., Rasmussen, C., Vajda, V., Ferrière, L., Feignon, J., Chenot, E., Perez-Cruz, L., Sato, H., Yamaguchi, K., IODP-ICDP Expedition 364 scientists, 2020. Geochemistry, geochronology and petrogenesis of Maya block granitoids and dykes from the Chicxulub impact crater, Gulf of México: Implications for the assembly of Pangea. Gondwana Res. 82, 128–150.

Zúñiga, S.J., Solari, L.A., Ortega-Obregón, C., 2020. Permian igneous clasts from the Matzitzi Formation, southern Mexico: isotopic constraints on the final amalgamation of Pangea. Geol. Soc. Lond. Spec. Publ. 503, 481–496. https://doi.org/10.1144/SP503-2019-238.